NASA/TM—2014-216676

Data Summary Report for the Open Rotor Propulsion Rig Equipped With F31/A31 Rotor Blades

David B. Stephens
Glenn Research Center, Cleveland, Ohio

November 2014

NASA STI Program . . . in Profile

Since its founding, NASA has been dedicated to the advancement of aeronautics and space science. The NASA Scientific and Technical Information (STI) program plays a key part in helping NASA maintain this important role.

The NASA STI Program operates under the auspices of the Agency Chief Information Officer. It collects, organizes, provides for archiving, and disseminates NASA's STI. The NASA STI program provides access to the NASA Aeronautics and Space Database and its public interface, the NASA Technical Reports Server, thus providing one of the largest collections of aeronautical and space science STI in the world. Results are published in both non-NASA channels and by NASA in the NASA STI Report Series, which includes the following report types:

- TECHNICAL PUBLICATION. Reports of completed research or a major significant phase of research that present the results of NASA programs and include extensive data or theoretical analysis. Includes compilations of significant scientific and technical data and information deemed to be of continuing reference value. NASA counterpart of peer-reviewed formal professional papers but has less stringent limitations on manuscript length and extent of graphic presentations.

- TECHNICAL MEMORANDUM. Scientific and technical findings that are preliminary or of specialized interest, e.g., quick release reports, working papers, and bibliographies that contain minimal annotation. Does not contain extensive analysis.

- CONTRACTOR REPORT. Scientific and technical findings by NASA-sponsored contractors and grantees.

- CONFERENCE PUBLICATION. Collected papers from scientific and technical conferences, symposia, seminars, or other meetings sponsored or cosponsored by NASA.

- SPECIAL PUBLICATION. Scientific, technical, or historical information from NASA programs, projects, and missions, often concerned with subjects having substantial public interest.

- TECHNICAL TRANSLATION. English-language translations of foreign scientific and technical material pertinent to NASA's mission.

Specialized services also include creating custom thesauri, building customized databases, organizing and publishing research results.

For more information about the NASA STI program, see the following:

- Access the NASA STI program home page at *http://www.sti.nasa.gov*

- E-mail your question to *help@sti.nasa.gov*

- Fax your question to the NASA STI Information Desk at 443–757–5803

- Phone the NASA STI Information Desk at 443–757–5802

- Write to:
  STI Information Desk
  NASA Center for AeroSpace Information
  7115 Standard Drive
  Hanover, MD 21076–1320

NASA/TM—2014-216676

Data Summary Report for the Open Rotor Propulsion Rig Equipped With F31/A31 Rotor Blades

David B. Stephens
Glenn Research Center, Cleveland, Ohio

National Aeronautics and
Space Administration

Glenn Research Center
Cleveland, Ohio 44135

November 2014

Acknowledgments

This report was funded by the NASA Environmentally Responsible Aviation (ERA) project and the NASA Fixed Wing (FW) project.

This work was sponsored by the Fundamental Aeronautics Program at the NASA Glenn Research Center.

Level of Review: This material has been technically reviewed by technical management.

Available from

NASA Center for Aerospace Information
7115 Standard Drive
Hanover, MD 21076–1320

National Technical Information Service
5301 Shawnee Road
Alexandria, VA 22312

Available electronically at http://www.sti.nasa.gov

Data Summary Report for the Open Rotor Propulsion Rig Equipped With F31/A31 Rotor Blades

David B. Stephens
National Aeronautics and Space Administration
Glenn Research Center
Cleveland, Ohio 44135

Abstract

An extensive wind tunnel test campaign was undertaken to quantify the performance and acoustics of a counter-rotating open rotor system. The present document summarizes the portion of this test performed with the so-called "Historical Baseline" rotor blades, designated F31/A31. It includes performance and acoustic data acquired at Mach numbers from take-off to cruise. It also includes the effect of propulsor angle of attack as well as an upstream pylon. This report is accompanied by an electronic data set including relevant acoustic and performance measurements for all of the F31/A31 data.

Data Rights

The data from the Historical Baseline blade set is nonproprietary and distribution is unrestricted, although the geometry of the blades is restricted by the International Traffic in Arms Regulations. The geometry is not presented in the present report.

Introduction

The oil shortages in the 1970s had a considerable impact on aeronautics research at NASA, leading to a number of energy efficiency related research projects as described in Reference 1. One major research area was the development of high-speed propellers for civil aviation, described in Reference 2. With the end of the oil crisis in the early 1980s, interest in the high-efficiency of advanced turboprop aircraft engines waned and development was essentially halted across the industry. A workable product incorporating counter-rotating propellers (now referred to as *open rotors*) had been demonstrated (Ref. 3) and the trade-off between fuel efficiency and noise had been established. Public perception also played a role, as propellers were perceived as old technology compared to the high-bypass turbofan engines which were entering service. The increase in fuel prices in the mid-2000s motivated new interest in fuel economy for aircraft and a computational effort at GE Global Research Center had produced several new designs for open rotors. In collaboration with the NASA Environmentally Responsible Aviation (ERA) project, an extensive test campaign on open rotors was conducted at NASA Glenn Research Center (GRC) in collaboration with GE Aircraft Engines from 2009 to 2012.

Several reports on specific subsets of the latest open rotor data have already been published (Refs. 4 to 7). The present document serves as a data report for the F31/A31 blade set, capturing the major results from the test and summarizing the large set of data that is available electronically. A brief description of the experimental equipment and instrumentation is provided, and the performance calculations are discussed. The full test matrix is given and a selection of results is presented.

Nomenclature

Note that this nomenclature applies to the Escort data in the archive associated with this paper. Therefore more symbols and abbreviations are included than are used in this report. Also note that units used in Escort were generally not metric and were also not a fundamental set. Values are called "corrected" if they are calculated using rpmc, or "effective" if they are calculated using effective thrust.

c_0	Speed of sound in freestream
f	Frequency, Hz
n	Rotation speed, revolutions per second rpm/60
p_{s0}	Tunnel freestream static pressure, psia
p_{t0}	Tunnel freestream total pressure, psia
rpm	Rotor revolutions per minute
rpmc	Corrected rpm, rpm/$\sqrt{\theta}$
A_A	Annulus area of propeller disk, ft^2
A_{CB}	Axially projected area of nacelle centerbody, ft^2
D	Rotor diameter, ft
J	Advance ratio, $60V_0$/rpm D
M_0	Freestream Mach number, V_0/c_0
PQA	Power coefficient, 550 $SHP/\rho\, n^3\, D^3\, A_A$
PQA/J^3	Propeller loading parameter, 550 $SHP/\rho\, V_0{}^3\, A_A$
Q	Rotor torque, ft-lb
SHP	Shaft horsepower, $\pi\, Q\, rpm/16500$
T	Rotor thrust, lbf
TQA	Thrust coefficient, $T/\rho n^2 D^2 A_A$
T_{s0}	Tunnel freestream static temperature, Rankine $T_{t0}/(1+ M_0{}^2/5)$
T_{t0}	Tunnel freestream total temperature, Rankine
SO	Shaft order, f/Ω
V_0	Freestream velocity, ft/s
α	Rig angle of attack, degrees
β_f	Forward rotor pitch angle, degrees
β_a	Aft rotor pitch angle, degrees
δ	Correction using tunnel freestream static pressure, p_{s0}/p_{ref}
ϕ	Sound emission angle measured from upstream axis of propulsor, radians
η	Efficiency, $V_0\, T/550\, SHP$
ρ	Air density, slugs/ft^3
θ	Correction value using tunnel freestream static temperature, T_{s0}/T_{ref}
Ω	Shaft rate, Hz

Experiment

The model test hardware simulates a counter rotating open rotor engine in a pusher configuration. The rotor blades being tested are powered by the Open Rotor Propulsion Rig (ORPR), a counter-rotating open rotor drive rig built for NASA by Boeing and GE in 1983 (Ref. 2). The ORPR was operated in both the 9- by 15-ft Low Speed Wind Tunnel (LSWT) and the 8- by 6-ft Supersonic Wind Tunnel (SWT) at GRC and a number of different rotor blade sets were tested for aerodynamic performance and acoustics. Comparisons of model scale acoustic data to the full-scale counter rotating engine flight test in the 1980s were found to be in good agreement (Ref. 8), therefore much of the overall test scheme was preserved from the earlier test.

Rotor Blades

New hubs for the ORPR were manufactured as part of the current test, with support for 12 forward rotor blades and 10 aft rotor blades. Blade fillers were also provided so that a *tare* configuration could be run, with tunnel airflow but without blades or shaft rotation. The pitch angle setting for both blade rows are manually adjustable. The "Historical Baseline" blade set used for the data in the present paper was designed and manufactured by GE and is designated as F31/A31. Dimensions and major parameters for F31/A31 are given in Table 1.This blade set represents a good aerodynamic design from the late 1980s, but was not acoustically optimized. An earlier set of F31/A31 blades had been tested by GE in their Cell 41 facility in the 1990s. A description of some of the open rotor testing done in Cell 41 is given in Reference 9. A new set was manufactured with modern composite materials and techniques for this test and provided a baseline to anchor data from advanced blade designs tested later in the campaign. The F31/A31 blade set was also used when checking out the rig and tunnel operability. Axial spacing between the two rotors was measured between the rotor blade pitch change axes. This parameter could be varied, but was set at 19.91 cm (7.84 in.) for the vast majority of this test. This spacing was referred to as "supermax." The blade set was designed to have equal torque applied to each rotor. The F31/A31 blades are shown in Figure 1.

Facilities

The test section of the 9- by 15-ft LSWT at GRC is 2.74 m high by 4.67 m wide (9- by 15-ft) and 8.72 m (28.6 ft) long. The test section walls have four 10.2 cm (4 in.) wide slots that run the length of the test section, which are designed to reduce tunnel wall effects. The flow is driven by three electric motors that can produce up to 65 MW (87,000 hp) and drive the tunnel velocity up to Mach 0.22. A flow conditioner provides a very low turbulence level in the center part of the test section. A description of the wind tunnel complex is given by Soeder (Ref. 10). Background noise levels were reported by Woodward et al. (Ref. 11) and the acoustic qualities of the facility were documented by Dahl and Woodward (Ref. 12). Note that the 9- by 15-ft LSWT is part of the return loop for the 8- by 6-ft SWT and therefore shares the same tunnel drive.

The 8- by 6-ft SWT is a high speed wind tunnel with velocity capabilities from Mach 0.27 to Mach 2.0. The test section is 2.44 m high by 1.83 m wide (8 ft by 6 ft) and 7.16 m (23.5 ft) long. The test section has bleed holes for boundary layer removal that are used when the tunnel is operated at transonic velocities. A description of the 8- by 6-ft SWT complex is given by Soeder (Ref. 13). Adjustments to the test section Mach number were made to account for blockage effects, as described in Reference 14.

Drive Rig

The NASA ORPR was used to power the open rotor blades in this test campaign. A description of the test rig as originally designed is in Reference 15. The rig consists of two counter rotating spools with a non-rotating center shaft. Each of the two counter rotating spools is attached to a two-stage air turbine on the aft end that can produce up to 560 kW (750 hp). The two air turbines are supplied by 2 MPa (300 psi) air heated to 90 °C (200 °F), and can be independently controlled using a feed-back system to drive the rotor speeds independently up to 8,000 rpm with an accuracy of ± 15 rpm. This drive rig was previously operated in the late 1980s and was refurbished during 2009 in order to correct any detrimental effects of long-term storage. The refurbishment activity consisted of a general inspection and rebuild of the mechanical components and construction of a new swept pylon. All instrumentation was inspected and replaced as necessary, including refurbishment of the forward and aft rotating force balances and installation of a modern telemetry system. The refurbished ORPR installed in the 9- by 15-ft LSWT is shown in Figure 2, with the acoustic instrumentation visible in the foreground. The ORPR installed in the 8- by 6-ft SWT is shown in Figure 3 with unsteady pressure instrumentation above.

During the early portion of the test campaign, excess noise was identified in the acoustic measurements. The measurements were compared with data previously acquired in the GE Cell 41 facility with F31/A31 blades and the drive rig turbine was identified as the likely culprit. A muffler was developed for the ORPR and was found to adequately mitigate this contamination, as documented in Reference 16. While the muffler was being developed, a large duct was used to carry the turbine exhaust outside the wind tunnel. Comparisons between the two exhaust noise mitigation systems show nearly comparable results, but the exhaust duct prevented the rig from going to angle of attack. The status of the turbine exhaust is provided for each data set. The muffler was used for all runs occurring on or after May 3, 2010.

Performance Instrumentation

The aerodynamic performance of the open rotor was quantified using rotating force balances mounted inside each rotor hub. These measured the steady thrust and torque produced by each rotor. Maximum loads on this instrumentation were limited to 2 kN (450 lbf) thrust per rotor and 680 Nm (500 ft-lb) torque. Accuracy determined by static test loads was approximately 1 percent of applied load for each component. The thrust and torque measurements provide means for calculating many performance parameters and were of critical importance. A number of corrections were used to convert the loads measured by the force balances into the loads caused by the rotor blades only. Brief summaries of the performance calculations are given in reports by Hughes and Gazzaniga (Ref. 17) and Stefko and Jeracki (Ref. 18), while the full details are contained in Reference 19. A summary is included here for convenience. A schematic of the forces involved is given in Figure 4.

The objective of the performance corrections is to isolate the thrust of both rotors, T_{net}. The tare run is used to obtain the drag on the rotor hubs, $D_{R,tare}$, which is calculated as follows. The rotor hub drag is composed of pressure drag due to uneven pressures on the upstream and downstream faces of the hub, plus the friction drag on the outer circumference of the hub. Both the pressure and friction loads are measured by the force balances during a tare run, giving $T_{bal,tare}$. A set of Kulite pressure transducers mounted on the upstream and downstream faces of each rotor hub measure only the pressure differential, which is multiplied by an area giving an internal pressure area term $PA_{int,tare}$ for each rotor face. These terms can be summed to give the total pressure drag force on the rotor faces. The friction drag can then be calculated as:

$$D_{R,tare} = T_{bal,tare} - \sum PA_{\text{int},tare} \, . \tag{1}$$

During the tare run the static pressure distribution on the forebody and afterbody of the rig nacelle is also measured and is denoted $p_{s,tare}$. This pressure distribution is measured by a large number of static pressure taps distributed axially and circumferentially around the forebody and afterbody.

When the rig is operating with blades, the apparent thrust T_{app} can be calculated from the thrust measured by the force balance T_{bal} by subtracting the load due to the pressure differential on the rotor hub faces and adding the friction drag,

$$T_{app} = T_{bal} - \sum PA_{\text{int}} + D_{R,tare} \, . \tag{2}$$

The rotor thrust changes the pressure field on the forebody and afterbody portions of the nacelle relative to the tare run. The static pressure distribution when the rig is operating with blades is denoted p_s. The axially projected area of the centerbody, dA_{CB}, is used to convert the pressure distribution into a drag force. The difference between this force when the rotor is powered and the tare configuration is

$$\Delta pA_{CB} = \int \left(p_s - p_{s0} \right) dA_{CB} - \int \left(p_{s,tare} - p_{s0} \right) dA_{CB} \, , \tag{3}$$

where ΔpA_{CB} is sometimes called a “buoyancy force”. Accounting for these nacelle forces, the net thrust is therefore

$$T_{net} = T_{app} - \Delta pA_{CB}\,. \tag{4}$$

This is also called the “effective” thrust.

9- by 15-Ft LSWT Acoustic Instrumentation

Acoustic instrumentation was a single Brüel and Kjær 4939 6.35 mm (1/4 inch) microphone with the standard UA-0385 bullet nose for making in-flow microphone measurements. This microphone was mounted on a linear traverse offset on a 1.52 m (5 ft) sideline from the centerline of the model, and can be seen in Figure 2. The sideline measurement covers the observation angles between 17.6° and 140° from the upstream axis of the fan. The microphone location geometry is given in Table 2 and a sketch of the geometry is shown in Figure 5. Emitted angles were calculated from geometric angles using the usual expression,

$$\theta_e = \theta_g - \sin^{-1}\left(M_0 \sin\theta_g\right), \tag{5}$$

which assumes linear propagation.

An RC Electronics DataMAX II data recorder was used to record 15-sec samples at 200 kHz, along with the once-per-revolution signals from the front and aft rotors. The Digital Acoustics Data System (DADS) software developed in the Acoustics Branch at GRC was used to process the recorded time series of pressures into sound pressure spectral densities (PSDs) with 12.2 Hz frequency bins. This software applied corrections for the microphone and bullet-nose sensitivity and directivity, resulting in “instrument corrected” spectra. Additionally, 1-ft lossless spectra were created by adding back losses due to atmospheric attenuation (Ref. 20) and amplitude reduction due to spherical spreading.

Background acoustic levels were documented during the tare runs as part of the model checkout process. This gives a measure of the background noise level in the wind tunnel including the scrubbing noise caused by airflow over the drive rig. Frequencies below 500 Hz have been omitted from results shown in this paper, due to background noise in the facility and limitations of the acoustic treatment below 350 Hz.

For portions of the 9- by 15-ft LSWT test, the traversing microphone was replaced by a linear array of flush mounted microphones embedded in a panel. These runs are specified in the provided data tables, but the data from this instrumentation are not discussed in this report. The microphone locations were the aft 16 of the 18 locations used for the traversing microphone.

8- by 6-ft SWT Unsteady Pressure Instrumentation

The unsteady pressure instrumentation for the 8- by 6-ft SWT portion of the test consisted of an aluminum plate with 17 flush-mounted XCS-093-15SG transducers made by Kulite Semiconductor axially aligned parallel to the model centerline. The transducers offer a 15 psi range and are temperature compensated. The calibration values provided with the instrumentation were used to convert the voltage output to unsteady pressure. These sensors were connected to a Precision Filter signal conditioning system and recorded by an RC Electronics DataMAX II. The pressure transducers were simultaneously sampled at 200 kHz in 15-sec long records. These records were processed into narrowband sound pressure level (SPL) spectra using DADS. These were converted to PSDs for this report by accounting for the bin width. The instrumented plate could be lowered by remote control from the tunnel ceiling to achieve various sideline distances from the model axis of rotation. A table of the geometry is in Table 3 . The emission angles were calculated using Equation (1). A schematic of the instrumentation relative to the model open rotor is shown in Figure 6. Most of the measurements were taken with the Kulite plate in

the stowed position against the test section ceiling and so are primarily of interest for the performance data acquired simultaneously. The plate was lowered only for specific test conditions while the DataMAX recorder was triggered for each reading. At Mach 0.4 with the plate in the stowed position, the sensors only span emitted angles between 46° and 90°. With the plate lowered to 0.78 rotor diameters above the model centerline and the freestream at Mach 0.78, the directivity spans emitted angles of 12° to 97° from upstream.

Test Matrix

The F31/A31 blade set served as the workhorse throughout the test campaign. The steady state data system used in the large test facilities at GRC is called Escort[1], and the test was divided up into several Escort programs. The F31/A31 blade set was run as part of three low speed programs (D069, D071 and D074) and one high speed program (D106). Each Escort program was divided into runs, with a new run number generated each time the tunnel was started. A run summary spreadsheet for each of the Escort programs is given as Table 5 to Table 8. The specific test readings points are listed in Table 9 to Table 12, one each for the four programs. Tare run readings are given in Table 13 and Table 14. The rig was tested across an extensive range of operating conditions, with blade pitch angles for the forward and aft blades ranging from the most closed forward/aft angles of 33.5°/35.7° at Mach 0.20 in the low speed tunnel to the most open angles of 64.4°/61.8° at Mach 0.85 in the high speed tunnel. The diameter for the blade pitch setting angle is given in Table 1. Powered rotation speeds ranged from 4000 rpmc at M = 0.20 up to 8265 rpmc at M = 0.85. The ORPR does not have an automated mechanism for changing the rotor blade pitch during a run, so only a limited number of iterations on blade pitch were practical during the course of testing. Changes to the rotor rpm at a fixed tunnel velocity provide an alternate method for changing the blade inflow angles.

Low Speed Test Matrix

The test campaign in the 9- by 15-ft LSWT was conducted to study the noise and performance of a modern open rotor at take-off and landing conditions. The majority of the low speed data available is at nominal take-off (NTO) and approach (APP) pitch angles while a limited amount of data was acquired at scaled take-off (STO) pitch angles. The specific forward/aft rotor pitch angles for the three conditions are given in Table 4.

The program D069 data includes the linear array acoustic instrumentation. All of D069 was acquired before the drive rig muffler was available and should therefore be considered contaminated with drive rig noise. None of the acoustic data from D069 is presented in the present report, but the linear array data may still be of interest and is available electronically. The D069 readings are given in Table 9. An acoustic barrier wall was installed for D069 run 49 to shield the microphone from drive rig turbine noise. During D069 checkout run 0P, the pylon sting was tested run without a pylon installed.

The scaled take-off measurements reported on in this paper were acquired during D071 and these readings are listed in Table 10. It should be noted that this data was taken with a temporary exhaust duct, as the drive rig muffler was not yet available. Some measurements of the rotor wakes were made using hot film anemometry, as noted in Table 6, but these measurements are not reported upon here. The bulk of the good low-speed F31/A31 data was acquired under Escort program D074, which was sponsored by the NASA ERA project. A pylon was added to the test campaign as part of D074 and angles of attack of 3° and 8° were investigated. A summary of the data acquired and the specific readings for each case is shown in Table 11. Additionally, a simplified acoustics shielding test was conducted, and those test conditions are also tabulated in Table 11. The muffler was implemented for D074 and D106.

A number of additional diagnostic methods were implemented during the D074 test. An Optinav Array 48 phased array microphone system was used to localize sound sources on the blades, as reported

[1] http://www.grc.nasa.gov/WWW/DSA/Escort_Data_Acquisition_Webpage/Escort_Webpage/Index.html

in Reference 21. Extensive particle image velocimetry (PIV) measurements were made of the flow between the rotors, as documented in Reference 22. Pressure sensitive paint measurements were also attempted, with modest results. These runs are documented in Table 7.

Virtually all data were taken with matched front and rear rotor rotation speeds. The exceptions are noted in Table 10 for program D071. The specific effect of non-unity rpm ratios on acoustics and performance will not be considered in this report. The rotor speeds and tunnel Mach number could be readily set during a run, so the primary variables changed between runs were the blade pitch angles. These were set by hand using precision inclinometers in a process that took approximately two hours. Along with the large number of blades to be tested, setting the blade pitch angles was the time limiting factor in mapping the overall system performance. An open rotor system as a commercial aircraft engine would utilize a pitch change mechanism to continually optimize the blade pitch angles for each operating condition.

The 9- by 15-ft LSWT tare run was made at the beginning of the test campaign during D069, and these measurements are tabulated in Table 13. It is worth noting that only five of the tare run points, RDGs 788, 802, 810, 814 and 818, are necessary for correcting essentially all of the powered data. The background acoustic data was used to correct the powered data to remove the tunnel background noise. Unfortunately, the tare run does not account for noise due to the drive rig turbines. This was handled with the implementation of the muffler previously described.

High Speed Test Matrix

The high speed test campaign was motivated primarily by the need to document the cruise performance of the advanced open rotor blades. The majority of the data was acquired at tunnel Mach numbers of 0.70 to 0.85, while a limited amount of data was acquired between Mach 0.27 and Mach 0.70. The higher tip Mach numbers encountered in this portion of the test meant more operability challenges and the blade stress levels were closely monitored. The nearfield unsteady pressure measurements could be used for estimating structural loading on the airframe or for predicting en route noise (Ref. 23), for example. A total of five blade pitch angles were run including some repeat data and a small set taken with the closer 18.34 cm (7.22 in.) “product” spacing between rotor blades, as noted in Table 12. Finally, during the run on August 25, 2011, the F31/A31 blade set was damaged when several screws holding the forebody together shook loose and convected through the rotors, affecting several blades. Due to the extensive data volume already obtained on F31/A31 and the effort required to manufacture replacements, it was decided not to re-build the blade set for additional testing.

A high speed tare run was part of D106 and is documented in Table 14. It includes many combinations of Mach number and plate height, although it should be noted that rotor data was acquired at Mach numbers up to 0.85 while tare data was only acquired to M = 0.80.

Results

Low and High Speed Isolated Rotor Dimensional Performance

Dimensional thrust and torque data are presented for the isolated rotor at all Mach numbers tested in Figure 7 to Figure 28, totaling eleven pairs of plots from Mach 0.20 to Mach 0.85. In cases where several blade pitch angles were tested at the same Mach number, multiple curves appear on the same plot. The most closed blade pitch angles are the approach condition (33.5°/35.7°), and it is seen that the front rotor is under more torque and generates more thrust. The nominal take-off pitch angle (40.1°/40.8°) is slightly more open and the thrust is nearly equal between front and aft rotors, while the torque is slightly higher on the front rotor. At scaled take-off (43.0°/43.5°) the aft rotor measures more thrust and torque. The scaled take-off pitch setting was also used for the lower speed runs in the 8- by 6-ft SWT (M = 0.27 to M = 0.45) and the blades were opened up further through 54.1°/53.5° and 60.5°/59.0° to finally 64.4°/61.8° as tunnel speeds up to M = 0.85 were tested. The effect of opening the pitch angles is

generally seen to shift the curves to lower rpm while keeping roughly the same slope. This seems to break down at the highest Mach numbers of 0.80 and 0.85, when presumably transonic effects become important. Interestingly, there are a few low power cases (first seen at M = 0.78 in Figure 23) where the front rotor is producing thrust while the aft rotor is still generating drag. The blade pitch angles were usually such that at low speed conditions the aft to forward torque ratio was less than one at low power and increased as the rotor shaft rate was increased. Note that these particular torque ratios may not be representative of an in-service product utilizing either a counter-rotating turbine or a gear system to drive the two rotors.

Low and High Speed Isolated Rotor Dimensionless Performance

A practical way to summarize the open rotor performance is through the use of non-dimensional propeller maps. The effective efficiency is shown in Figure 29, the propeller loading parameter is shown in Figure 30 and the torque ratio is plotted against advance ratio in Figure 31. These three plots show data from both low and high speed wind tunnels. It can be seen that a peak efficiency of 85.8 percent was recorded at Mach 0.67. GE Aviation reported that performance measurements acquired during this wind tunnel test were in good agreement with their Cell 41 historic data. The propeller loading parameter collapses the majority of the data for each pitch angle except for tunnel speeds of Mach 0.85.

Low and High Speed Installed Rotor Dimensionless Performance

The effects of both a pylon and rig angle of attack were tested in the low speed tunnel. For brevity, only the data from NTO pitch angles are shown. Dimensionless plots of efficiency, propeller loading and torque ratio are shown in Figure 32 through Figure 40 for rig angles of attack of 0°, 3° and 8°. Each plot shows both “isolated” and “pylon” data. Neither the pylon nor rig pitch angle has a large effect individually, but the combination is seen to significantly increase the load on rear rotor while decreasing the load on the front rotor.

Low Speed Acoustics

The acoustic measurements were converted to pressure spectral densities, as previously discussed. An example of a typical instrument-corrected sound sample is given in Figure 41 and Figure 42. The same data is represented in terms of shaft order in Figure 43. Much of the tone content seen in these figures is found at expected shaft orders (*SO*) for interaction tones, calculated as sums of integer multiples of the front (*m*) and rear (*n*) blade counts when the shaft speeds are equal,

$$SO(m,n) = 12m + 10n\ . \tag{6}$$

These shaft orders are given in Table 15. The large number of tones and the complicated directivity of the open rotor system make inspection of individual spectra of limited value.

The directivity of some of the loudest tones produced by the open rotor is shown in Figure 44 through Figure 49. These data show the instrumented corrected and background (tare) subtracted noise levels measured along a 5-ft sideline and converted to emission angles. The total overall sound pressure level (OASPL) integrated over frequencies between 500 Hz and 50 kHz is also shown as the top curve (dark blue diamonds). Figure 44 through Figure 46 show the isolated rotor at zero AoA for pitch angles of NTO, APP and STO. Figure 47 though Figure 49 use the NTO pitch angle to show the effect of AoA only, the effect of the pylon only, and then the combined effect of both AoA and Pylon. The tone amplitudes were quantified by integrating the spectra at a few frequencies around each shaft order where a tone was anticipated. The specific tones that are loudest change based on operating and test conditions, but the selection shown here were generally among the loudest. There did not seem to be a case where a particular tone contributed dramatically more than any other. It can be seen that generally the first

forward and aft fundamental blade passage tones (SO12 and SO10, respectively) have the typical parabolic shape that is expected for propeller tones with a peak roughly broadside to the rotor. The interaction tones on the other hand have a more complicated pattern that is clearly under-resolved by the 18 spatial measurement locations. The blade rate tones have the biggest contribution at approach pitch angles, and these diminish as the blade angle opens up. At scaled take-off, the interaction tones dominate the directivity. It is of interest to note the change in the spectra due to the addition of the pylon. The primary difference is a substantial increase in the front rotor blade passing frequency (BPF) tone, especially at forward and aft angles with increases of more than 15 dB for SO12 tones at some directivity angles.

The spatially integrated sound metric overall power level (OAPWL) was calculated using DADS. The usual expression for finding the sound power from measurements of pressure made on the surface of a sphere assuming symmetry along the axis of the propulsor is given as Equation (7)

$$P = 2\pi \int_0^{\pi} \frac{\overline{p^2(\phi)}}{\rho_0 c_0} r^2 \sin\phi \, d\phi, \tag{7}$$

where ϕ is the sound emission angle in radians, measured from upstream.

The software begins with the sideline measurements, assumes the source is axisymmetric and integrates the sound pressure level over a surface from the upstream-most angle measured to the downstream-most. The computed OAPWL is shown in Figure 50 to Figure 53 for NTO and APP pitch angles, with and without the pylon. Comparing the curves for AoA=0 in Figure 50 and Figure 51, it is seen that both NTO and APP show nearly the same OAPWL at low and high power, but the NTO pitch angle is quieter at middle power settings. The effect of angle of attack of 8° is to increase OAPWL by around 0.5 dB at low power and 1.5 dB at high power. The decibel increase in the presence of the pylon is greater at low power than at high power for both blade pitch angles. One possibility is that the propeller tends to align the flow with the pylon, effectively improving its own inflow. It is known that noise levels from the approaching rotor blade at non-zero AoA results in higher localized loading of that blade which, in turn, locally increases the perpendicularly-radiating noise from that approaching rotor. This effect was documented using a microphone traversed in a polar arc around the open rotor (Ref. 24).

A major end product of the acoustic data was the system level noise analysis known as Effective Perceived Noise Level (EPNL). Publications describing this analysis and the results include References 4 25. During this process, the data is converted to 1/3rd octave band, so many details are lost. The EPNL calculation is also subject to the specific scaling of the wind tunnel data to a certain size and thrust capacity engine for a specific aircraft and to the trajectory that aircraft flies. For these reasons EPNL is not considered in this report.

High Speed Unsteady Pressure Results

The extremely close measurement location used in the high speed portion of this test (less than two diameters at most) leads to the conclusion that the data must be considered as near field unsteady pressure measurements, containing a combination of acoustic and hydrodynamic pressures. A sample of the spectral data is shown in Figure 55 and Figure 56, where the different lines show simultaneous measurements made at two sensor locations, one over each rotor. Sensor 9 is directly over the aft rotor, and the aft rotor blade rate and harmonics are seen to dominate. Sensor 12 is roughly over the forward rotor, and the spectrum is shown to be likewise dominated by forward rotor tones. The tare spectra are much lower than the tones, but may be slightly higher than the broadband of the powered spectra for frequencies below about 3200 Hz.

The dominance of the rotor blade rate tones is immediately apparent in the directivity plots, shown as Figure 57 to Figure 62. These figures present measurements made with a sensor plate height of 16.8 in. above the model centerline. The plots show the blade rate tone directivities along a sideline, along with

the OASPL integrated between 500 Hz and 50 kHz. The sideline direction has been reversed so that upstream is to the left, to correspond with the directivity plots from the low speed data. The emitted angle for each tone (forward and aft) can be calculated with respect to the appropriate rotor, which will cause the two peaks to collapse as demonstrated in Reference 7. This representation would be appropriate when considering an observer far from the model, at a distance where the rotor spacing is relatively small.

Conclusions

A summary of the main results from the F31/A31 data set have been presented. A peak efficiency of 85.8 percent was recorded at Mach 0.67. The acoustic penalty measured with the pylon installed was up to 3.5 dB at low power and around 0.5 dB at high power on a sound power level basis. The data from the 9- by 15-ft LSWT showed a profusion of tones, while the nearfield unsteady pressured data recorded at cruise Mach numbers was dominated by the blade rate tones from the two rotors. This report is an overview of the available data and readers may wish to obtain the electronic data set associated with this report for their own analysis.

References

1. Bowles, Mark D.: The “Apollo” of Aeronautics: NASA's Aircraft Energy Efficiency Program, 1973–1987. SP–2009–574, 2010. http://ntrs.nasa.gov
2. Hager, Roy D.; and Vrabel, Deborah: Advanced Turboprop Project. NASA SP–495, 1988. http://ntrs.nasa.gov
3. Harris, Robert W.; and Cuthbertson, R.D.: UDF™/727 Flight Test Program. AIAA–87–1733, 1987.
4. Berton, Jeffrey J.: Empennage Noise Shielding Benefits for an Open Rotor Transport. NASA/TM—2012-217218 (AIAA–2011–2764), 2012. http://ntrs.nasa.gov
5. Stephens, David B.; and Envia, Edmane: Acoustics Shielding for a Model Scale Counter-Rotation Open Rotor. NASA/TM—2012-217227 (AIAA–2011–2940), 2012. http://ntrs.nasa.gov
6. Elliott, David M.: Initial Investigation of the Acoustics of a Counter-Rotating Open Rotor Model With Historical Baseline Blades in a Low-Speed Wind Tunnel. NASA/TM—2012-217258 (AIAA–2011–2760), 2012. http://ntrs.nasa.gov
7. Stephens, David B.: Nearfield Unsteady Pressures at Cruise Mach Numbers for a Model Scale Counter-Rotation Open Rotor. NASA/TM—2012-217672 (AIAA–2012–2264), 2012. http://ntrs.nasa.gov
8. Woodward, Richard P.; Loeffler, Irvin J.; and Dittmar, James H.: Measured Far-Field Flight Noise of a Counterrotation Turboprop at Cruise Conditions. NASA TM–101383, 1989. http://ntrs.nasa.gov
9. Janardan, B.A., et al.: Scale Model Acoustic Testing of Counterrotating Fans. AIAA 1988–2057, 1988.
10. Soeder, Ronald H.: NASA Lewis 9- by 15-Foot Low-Speed Wind Tunnel User Manual. NASA TM–106247, 1993. http://ntrs.nasa.gov
11. Woodward, R.P., et al.: Background Noise Levels Measured in the NASA Lewis 9- by 15-Foot Low-Speed Wind Tunnel. AIAA–95–0720, 1995.
12. Dahl, Milo D.; and Woodward, Richard P.: Comparison Between Design and Installed Acoustic Characteristics of NASA Lewis 9- by 15-Foot Low-Speed Wind Tunnel Acoustic Treatment. NASA TP–2996, 1990. http://ntrs.nasa.gov
13. Soeder, Ronald H.: NASA Lewis 8- by 6-Foot Supersonic Wind Tunnel User Manual. NASA TM–105771, 1993. http://ntrs.nasa.gov
14. Stefko, George L.; and Jeracki, Robert J.: Porous Wind Tunnel Corrections for Counterrotation Propeller Testing. NASA/TM—1988-100873 (AIAA–88–2055), 1988. http://ntrs.nasa.gov
15. Delaney, B., et al.: A Model Propulsion Simulator for Evaluating Counterrotating Blade Characteristics. SAE 861715, 1986.

16. Stephens, David B.: Acoustic Performance of Drive Rig Mufflers for Model Scale Engine Testing. NASA/TM—2013-217885, 2013. http://ntrs.nasa.gov
17. Hughes, Christopher E.; and Gazzaniga, John A.: Summary of Low-Speed Wind Tunnel Results of Several High-Speed Counterrotation Propeller Configurations. AIAA 88–3149, 1988. http://ntrs.nasa.gov
18. Stefko, George L.; and Jeracki, Robert J.: Wind-Tunnel Results of Advanced High-Speed Propellers at Takeoff, Climb, and Landing Mach Numbers. NASA TM–87030, 1986. http://ntrs.nasa.gov
19. SAE International: Propeller Propfan In-Flight Thrust Determination (Stabilized Type). SAE AIR 4065, 2012.
20. Acoustical Society of America: Method for Calculation of the Absorption of Sound by the Atmosphere. ANSI S1.26-1995, 1995.
21. Horváth, Csaba; Envia, Edmane; and Podboy, Gary G.: Limitations of Phased Array Beamforming in Open Rotor Noise Source Imaging. AIAA 2013–2098, 2013.
22. VanZante, Dale E.; and Wernet, Mark P.: Tip Vortex and Wake Characteristics of a Counterrotating Open Rotor. NASA/TM—2012-217713 (AIAA 2012–4039), 2012. http://ntrs.nasa.gov
23. Dittmar, J.H.: An Estimate of the Enroute Noise of an Advanced Turboprop Airplane. NASA TM–87302, 1986. http://ntrs.nasa.gov
24. Woodward, Richard P.: Noise of a Model High Speed Counterrotation Propeller at Simulated Takeoff/Approach Conditions (F7/A7). NASA TM–100206 (AIAA–87–2657), 1987. http://ntrs.nasa.gov
25. Guynn, Mark D., et al.: Initial Assessment of Open Rotor Propulsion Applied to an Advanced Single-Aisle Aircraft. NF1676L–12112 (AIAA 2011–7058), 2011.

TABLE 1.—MAJOR F31/A31 PARAMETERS

Parameter	Value
Forward rotor diameter, cm (in.)	65.18 (25.66)
Aft rotor diameter, cm (in.)	62.97 (24.79)
Forward hub diameter, cm (in.)	26.56 (10.46)
Aft hub diameter, cm (in.)	24.65 (9.70)
Pitch setting diameter (both rotors), cm (in.)	45.79 (19.21)
Design forward tip speed, m/s (ft/s)	228.6 (750)
"Supermax" rotor spacing, cm (in.)	19.91 (7.84)
"Product" rotor spacing, cm (in.)	18.34 (7.22)
Design torque ratio	1
Aft clipping	0
Full-scale max climb disk loading, kW/m^2 (hp/ft^2)	802.7 (100)
Scale factor	5

TABLE 2.—GEOMETRY FOR THE 9- BY 15-ft LSWT MICROPHONE ACOUSTIC MEASUREMENTS, MACH 0.20 AND 19.91 cm (7.84 in.) ROTOR SPACING

	Aft rotor centered			Forward rotor centered		
Stop no.	Streamwise location	Geometric angle	Emission angle	Streamwise location	Geometric angle	Emission angle
1	–5.95	140.0	132.6	–6.60	142.9	135.9
2	–5.00	135.0	126.9	–5.65	138.5	130.9
3	–3.83	127.5	118.3	–4.48	131.9	123.3
4	–2.88	119.9	110.0	–3.53	125.2	115.8
5	–2.08	112.6	101.9	–2.73	118.7	108.6
6	–1.34	105.0	93.9	–1.99	111.7	101.0
7	–0.66	97.5	86.1	–1.31	104.7	93.6
8	0.00	90.0	78.5	–0.65	97.4	86.0
9	0.66	82.5	71.0	0.01	89.9	78.4
10	1.34	75.0	63.9	0.69	82.2	70.8
11	2.08	67.4	56.8	1.43	74.1	63.0
12	2.88	60.1	50.1	2.23	66.0	55.5
13	3.83	52.5	43.4	3.18	57.6	47.9
14	5.00	45.0	36.9	4.35	49.0	40.3
15	6.52	37.5	30.5	5.87	40.4	33.0
16	8.66	30.0	24.3	8.01	32.0	25.9
17	12.08	22.5	18.1	11.43	23.6	19.0
18	15.72	17.6	14.2	15.07	18.4	14.7

TABLE 3.—GEOMETRY FOR THE 8- BY 6-ft SWT KULITE SENSOR LOCATIONS FOR 0.65 DIAMETER PLATE HEIGHT ABOVE MODEL CENTERLINE, MACH 0.78 AND 19.91 cm (7.84 in.) ROTOR SPACING

Hplate..... 16.74	Mach 0.78	Rotor spacing 7.84

	Aft rotor centered			Forward rotor centered		
Sensor no.	Streamwise location	Geometric angle (θ_g), degrees	Emission angle (θ_e), degrees	Streamwise location	Geometric angle (θ_g), degrees	Emission angle (θ_e), degrees
1	–18.4	137.7	106.0	–26.2	147.5	122.7
2	–15.3	132.4	97.3	–23.1	144.1	116.9
3	–13.4	128.7	91.2	–21.2	141.8	112.9
4	–11.6	124.7	84.8	–19.4	139.3	108.7
5	–9.2	118.8	75.7	–17.0	135.5	102.4
6	–7.4	113.8	68.3	–15.2	132.3	97.1
7	–5.8	109.1	61.6	–13.6	129.2	92.0
8	–2.8	99.5	49.2	–10.6	122.4	81.3
9	0.0	90.0	38.7	–7.8	115.1	70.2
10	2.8	80.5	30.2	–5.0	106.8	58.4
11	5.8	70.9	23.4	–2.0	96.9	46.2
12	7.4	66.2	20.6	–0.4	91.5	40.3
13	9.2	61.2	18.1	1.4	85.4	34.3
14	11.6	55.3	15.4	3.8	77.3	27.8
15	13.4	51.3	13.8	5.6	71.6	23.9
16	15.3	47.6	12.4	7.5	66.0	20.5
17	18.4	42.3	10.6	10.6	57.8	16.5

TABLE 4.—BLADE SETTING ANGLES FOR 9- BY 15-ft LSWT TESTING

Setting	Angles
Nominal take-off (NTO)	40.1°/40.8°
Scaled take-off (STO)	43.0°/43.5°
Approach (APP)	33.5°/35.7°

TABLE 5.—D069 F31/A31 RUN SUMMARY

Run no.	Escort program	RDGs.	Config no.	Test type	Tunnel Mach	AoA	Fwd rotor β angle	Aft rotor β angle	Test date	Comments
0A	D069	76-89	Checkout Run 1	Checkout	0	0	41.1	40.3	24-Sep-09	
0B	D069	94-111	Checkout Run 2	Checkout	0	0	41.1	40.3	25-Sep-09	
0C	D069	112-133	Checkout Run 3	Checkout	0	0	41.1	40.3	28-Sep-09	
0D	D069	134-162	Checkout Run 4	Checkout	0	0	41.1	40.3	29-Sep-09	
0E	D069	163-196	Checkout Run 4	Checkout	.05,-.2	0	41.1	40.3	29-Sep-09	
0F	D069	197-229	Checkout Run 5	Checkout	0.2	0	41.1	40.3	1-Oct-09	
0G	D069	230-244	Checkout Run 7	Checkout	0.2	0	41.1	40.3	1-Oct-09	
0H	D069	245-279	Checkout Run 7	Checkout	0.2	0	41.1	40.3	5-Oct-09	
0I	D069	281-313	Checkout Run 9	Checkout	0.2	0	41.1	40.3	6-Oct-09	
0J	D069	314-332	Checkout Run 10	Checkout	0.2	0	41.1	40.3	7-Oct-09	
0K	D069	333-355	Checkout Run 11	Checkout	0.2	0	41.1	40.3	8-Oct-09	
0M	D069	861-878	Checkout Run 12 B	Checkout	0.2	0	41.1	40.3	23-Oct-09	
0N	D069	879-901	Checkout Run 14	Checkout	0.2	0	41.1	40.3	23-Oct-09	
0O	D069	903-908	Checkout Run 15	Checkout	0.2	0	41.1	40.3	26-Oct-09	
0P	D069	909-924	Checkout Run 15	Checkout	0.2	0,8	41.1	40.3	26-Oct-09	
0Q	D069	923-941	Checkout Run 16	Checkout	0.2	0,8	41.1	40.3	26-Oct-09	
0R	D069	942-949	Checkout Run 18	Checkout	0.2	0	41.1	40.3	26-Oct-09	
2	D071	2003-2021	11A	Performance	0.2	0	40.1	40.8	27-Oct-09	
3	D071	2022-2039	11B	Performance	0.2	0	43.0	43.5	27-Oct-09	
4	D071	2043-2062	12A	Acoustic	0.2	0	43.0	43.5	28-Oct-09	
5	D071	2063-2118	12B	Acoustic	.18,.2	0	40.1	40.8	28-Oct-09	
49	D069	1115-1154	12LA WI	Acoustic	.18,.2,.22	0,3,8,-3	0.0	0.0	10-Dec-09	Linear array
50	D069	1155-1192	12LA WO	Acoustic	.18,.2,.22	0,3,8,-3	0.0	0.0	10-Dec-09	Linear array

TABLE 6.—D071 RUN SUMMARY

Run no.	Escort program	RDGs.	Configuration no.	Test Type	Tunnel Mach	AoA	Fwd rotor β angle	Aft rotor β angle	Test date	Comments
67	D071	4220-4249	12C	Acoustic	0.2	0	40.1	40.8	9-Mar-10	
68	D071	4251-4256	13A	Aborted	0.2	0	33.1	36.3	9-Mar-10	Target torque ratio not met.
68b	D071	4257-4273	13A	Acoustic	0.2	0	33.5	35.7	9-Mar-10	Wrapped exit duct
69	D071	4274-4298	12D	Acoustic	0.2	0	43.0	43.5	10-Mar-10	Wrapped exit duct
70	D071	4299-4319	121A	Hot Film	0.2	0	43.0	43.5	10-Mar-10	Wake rake 0° HW downstream
71	D071	4320-4341	121A	Hot Film	0.2	0	43.0	43.5	11-Mar-10	Wake rake 0° HW Mid.
72	D071	4342-4416	122A	Hot Film	0.2	0	40.1	40.8	11-Mar-10	Wake rake 0° HW Mid.
73	D071	4417-4472	123A	Hot Film	0.2	0	33.5	35.7	12-Mar-10	Wake rake 0° HW downstream

TABLE 7.—D074 RUN SUMMARY

Run no.	Escort program	RDGs.	Configuration no.	Test type	Tunnel Mach	AoA	Fwd rotor β angle	Aft rotor β angle	Test date	Comments
202	D074	75-100	PA PYL	Phased array	0.20,0.22	0,-3,-8	40.1	40.8	23-Jul-10	TO Nom
203	D074	101-125	PA PYL	Phased array	0.20,0.22	0,-3,-8	33.5	35.7	23-Jul-10	App
204	D074	126-150	PA ISO	Phased array	0.20,0.22	0,-3,-8	33.5	35.7	26-Jul-10	App re: Run 68b on 3/9/10
205	D074	151-176	PA ISO	Phased array	0.20,0.22	0,-3,-8	40.1	40.8	26-Jul-10	TO Nom re: Run 5 on 10/28/09
213	D074	345-377	FF PYL	Acoustic	0.2	0,3,8	40.1	40.8	2-Aug-10	TO Nom
214	D074	378-416	FF PYL	Acoustic	0.20,0.22	0,3,8	33.5	35.7	3-Aug-10	App
215	D074	417-456	FF ISO	Acoustic	0.20,0.22	0,3,8	33.5	35.7	3-Aug-10	App
216	D074	457-499	FF ISO	Acoustic	0.20,0.22	0,3,8	40.1	40.8	4-Aug-10	TO Nom
217	D074	500-514	FF ISO wall fwd	Acoustic	0.20,0.22	0	40.1	40.8	5-Aug-10	Semi-infinite barrier wall
218	D074	515-531	FF ISO wall aft	Acoustic	0.20,0.22	0	40.1	40.8	5-Aug-10	Semi-infinite barrier wall
219	D074	532-535	PSP ISO aft	PSP	0.2	0	40.1	40.8	9-Aug-10	Checkout run
220	D074	536-556	PSP ISO aft	PSP	0.2	0	40.1	40.8	10-Aug-10	
221	D074	557-579	PSP ISO aft	PSP	0.2	0	40.1	40.8	11-Aug-10	
222	D074	580-619	PSP ISO aft	PSP	0.2	0	40.1	40.8	12-Aug-10	
223	D074	620-649	PSP PYL fwd	PSP	0.2	0	40.1	40.8	13-Aug-10	
224	D074	650-654	PIV ISO	PIV	0.037	0	40.1	40.8	20-Aug-10	Wing blowers, seeder check
225	D074	655-668	PIV ISO	PIV	0.2	0	40.1	40.8	20-Aug-10	Computer issues
226	D074	669-824	PIV ISO	PIV	0.2	0	40.1	40.8	23-Aug-10	TO nom
227	D074	825-890	PIV ISO	PIV	0.2	0	33.5	35.7	25-Aug-10	App
230	D074	1051-1067	FF ISO wall	Acoustic	0.20,0.22	0	40.1	40.8	7-Sep-10	Finite barrier wall forward
231	D074	1068-1084	FF ISO wall	Acoustic	0.20,0.22	0	40.1	40.8	7-Sep-10	Finite barrier wall aft

TABLE 8.—D106 RUN SUMMARY

Run no.	Escort program	RDGs.	Configuration no.	Test type	Tunnel Mach	AoA	Fwd rotor β angle	Aft rotor β angle	Test Date	Comments
5	D106	707-718	CK OUT 1		0.33	0	43.0	43.5	28-Feb-11	Run aborted
6	D106	719-746	CK OUT 2		0.27-0.36	0	43.0	43.5	1-Mar-11	
7	D106	747-782	CK OUT 3	Acoustic	0.27-0.45	0	43.0	43.5	2-Mar-11	
8	D106	783-810	CK OUT 4		0.4,0.45	0	54.1	53.5	3-Mar-11	
9	D106	811-834	CK OUT 5	Acoustic	0.60,0.67	0	54.1	53.5	9-Mar-11	
10	D106	1057-1066	CK OUT 6		0.6	0	54.1	53.5	6-Apr-11	
11	D106	1333-1352	CK OUT 7	Acoustic	0.6	0	54.1	53.5	3-Jun-11	
12	D106	1353-1360	CK OUT 8		0.6	0	54.1	53.5	6-Jun-11	
13	D106	1361-1364	CK OUT 9	Acoustic	0.6	0	54.1	53.5	7-Jun-11	No acoustic readings made
14	D106	1365-1374	CK OUT 10	Acoustic	0.6	0	54.1	53.5	8-Jun-11	No acoustic readings made
15	D106	1375-1398	CK OUT 11	Acoustic	0.6,0.67	0	54.1	53.5	9-Jun-11	
16	D106	1420-1443	CK OUT 12	Acoustic	0.67-0.73	0	54.1	53.5	10-Jun-11	
17	D106	1444-1478	CK OUT 13	Acoustic	0.67-0.78	0	60.5	59.0	10-Jun-11	
18	D106	1479-1522	CK OUT 14	Acoustic	0.73-0.85	0	64.4	61.8	11-Jun-11	
38	D106	2841-2924	GE 20	Acoustic	0.67-0.85	0	60.5	59.0	8-Aug-11	
39	D106	2925-2994	GE 21	Acoustic	0.73-0.85	0	64.4	61.8	9-Aug-11	
40	D106	2996-3071	GE 22	Acoustic	0.73-0.85	0	62.9	60.5	9-Aug-11	
47	D106	3390-3408	GE 29	Acoustic	0.73-0.78	0	64.4	61.8	17-Aug-11	
62	D106	3838-3943	GE 30	Acoustic	0.73-0.85	0	64.4	61.8	25-Aug-11	Product spacing, second incident

TABLE 9.—D069 F31/A31 READING LIST—ACOUSTIC DATA
ACQUIRED WITHOUT EXHAUST MUFFLER
[D069 F31/A31 No Muffler]

	40.1/40.8	40.1/40.8	41.1/40.3		41.1/40.3, pylon sting	
	Aero, linear array, barrier wall	Aero, linear array	Aero	Acoustic	Aero	Acoustic
M = 0.20	1123	1163	868	869	912	[a]913
	1124	1164	870	871	915	[a]916
	1125	1165	883	[a]884	927	928
	1126	1166	885	[a]886	930	931
	1127	1167				
	1128	1168				
	1129	1169				
	1130	1170				
	1131	1171				
	1132					
	1133					
	1134					
M = 0.18	1118	1158				
	1119	1159				
	1120	1160				
		1161				
M = 0.22	1150	1187				
	1151	1188				
	1152	1189				
		1190				
AoA = 3	1137	1174				
	1138	1175				
	1139	1176				
AoA = 8	1142	1179	872	873	917	[a]918
	1143	1180	874	875	919	[a]920
	1144	1181	888	[a]889	934	935
			890	[a]891	936	937
AoA = –3	1147	1184				

[a] Camera box on upper south wall, instead of acoustic box

TABLE 10.—D071 F31/A31 READING LIST—ACOUSTIC DATA
ACQUIRED WITH TURBINE EXHAUST DUCT
[D071 F31/A31—turbine exhaust duct]

	33.1/36.3	33.5/35.7		40.1/40.8		43.0/43.5	
	Aero	Aero	Acoustic	Aero	Acoustic	Aero	Acoustic
M = 0.20	4254	4260	4261	4226	4227	4278	
		4262	4263	4228	4229	4279	4280
		4264	4265	4230	4231	4281	4282
		4266	4267	4232	4233	[a]4283	[a]4284
		4270	4271	4234	4235	4285	4286
				[a]4236	[a]4237	4287	4288
				4238	4239	[a]4289	[a]4290
				4240	4241	4291	4292
				[a]4242	[a]4243	[a]4293	[a]4294
				4244	4245	[a]4295	[a]4296
				4246	4247		

[a] rpm1!=rpm2

TABLE 11.—D074 F31/A31 READING LIST—ACOUSTIC DATA ACQUIRED WITH EXHAUST MUFFLER

(a) D074 F31/A31

	40.1/40.8 with pylon		40.1/40.8 no pylon		33.5/35.7 no pylon		33.5/35.7 with pylon	
	Aero	Acoustic	Aero	Acoustic	Aero	Acoustic	Aero	Acoustic
M = 0.20	351	352	460		420		381	382
	353		461	462	421	422	383	384
	354	355	463	464	423	424	385	386
	356	357	465	466	425	426	387	388
	358	359	467	468	427	428	389	390
	360	361	469	470	429	430		
			471	472				
AoA = 3	364	365	475	476	433	434	393	394
	366	367	477	478	435	436	395	396
	368	369	479	480	437	438	397	398
AoA = 8	372	373	483	484	441	442	401	402
	374	375	485	486	443	444	403	404
			487	488	445	446	405	406
M = 0.22			491	492	449	450	409	410
			493	494	451	452	411	412
			495	496	453	454	413	414

(b) D074 F31/A31 with barrier wall

	40.1/40.8 long wall forward		40.1/40.8 long wall aft		40.1/40.8 short wall forward		40.1/40.8 short wall aft	
	Aero	Acoustic	Aero	Acoustic	Aero	Acoustic	Aero	Acoustic
M = 0.20	503	504	520	521	1055	1056	1072	1073
	505	506	522	523	1057	1058	1074	1075
M = 0.22	509	510	526	527	1062	1063	1079	1080
	511	512	528	529	1064	1065	1081	1082

TABLE 12.—D106 F31/A31 READING LIST—ACOUSTIC DATA
ACQUIRED WITH EXHAUST MUFFLER

D106 F31/A31

	43.0/43.5	54.1/53.5	60.5/59.0	[c]60.5/59.0	62.9/60.5	64.4/61.8	[c]64.4/61.8	[d]64.4/61.8
M = 0.27	728							
	729							
	731							
	732							
	733							
	734							
	735							
	[a]766							
M = 0.36	738							
	739							
	740							
	741							
	742							
	743							
	774							
	[a]775							
M = 0.40	750							
	751							
	752							
	[a]753							
M = 0.45	762	788						
	763	789						
		790						
		791						
		792						
		[b]793						
		[b]794						
M = 0.60		819						
		820						
		821						
		822						
		[a]823						
		1381						
		1382[a]						
		1387						
M = 0.67		1390	1463	2909				
		1392	1464	2910				
		1393	[a]1465	[a]2911				
		1394	1470	[a]2916				
		[a]1429	[a]1471	2921				
			1476	2922				
M = 0.73		1435	1452	2890	2998	[a]1506	2928	3889
		1436	1453	2891	2999	[a]1511	2929	3890
		1437	[a]1454	2892	3000	[a]1516	2930	3891
			1459	[a]2893	[a]3001		2931	3892
			1460	2898	[a]3007		2932	3893
				[a]2899	3012		3393	3894
				2905	3013		3394	
				2906	3014		3395	
							3396	

TABLE 12.—D106 F31/A31 READING LIST—ACOUSTIC DATA
ACQUIRED WITH EXHAUST MUFFLER

D106 F31/A31

	43.0/43.5	54.1/53.5	60.5/59.0	[c]60.5/59.0	62.9/60.5	64.4/61.8	[c]64.4/61.8	[d]64.4/61.8
M = 0.78			1447	2844	3017	[a]1492	[a]2935	3841
			1448	2845	3018	[a]1497	[a]2940	3842
			1449	2846	3019	[a]1502	[a]2945	[a]3843
				[a]2847	[a]3020		[a]2950	[a]3848
				2852	3025		[a]2955	[a]3853
				[a]2853	[a]3026		2960	3858
				2860	3031		2961	3859
				2861	3032		[a]2962	[a]3860
							3399	3877
							3400	3878
							3401	3879
							3402	[a]3880
							3403	3885
							3404	3886
							3405	
							3406	
M = 0.80				2864	3035	1488	2970	3897
				[a]2865	3036	1489	2971	3898
				2870	3037		2972	3899
				[a]2871	[a]3038		2973	3900
				2876	3043		2974	3901
				2877	3044		2975	3902
				2878	[a]3045		2976	3903
				2879	3050		2977	3904
M = 0.85				2882	3054	1482	2980	3907
				2883	3055	1483	2981	3908
				2884	3056	1484	2982	3909
				2885	[a]3057	1485	2983	3910
				2886	3063		2984	3911
				2887	3064		2985	3912
					[a]3065		2986	3913
							[a]2987	3914
							2992	3915
								3916
								[a]3917
								3921
								3922

[a] Kulite plate survey taken at this condition; [b] Indicates angle of attack; [c] Indicates repeat run; [d] Indicates product spacing

TABLE 13.—9- BY 15-ft LSWT TARE READINGS

	D069 tare run (no blades)		
	AoA	Aero	Acoustic
M = 0.10	0	764	765
M = 0.15	0	773	774
	–3	775	776
	–4	777	778
	3	780	781
	4	782	783
	8	784	785
M = 0.18	0	787	[a]788
	–3	789	790
	–4	791	792
	3	794	795
	4	796	797
	8	797	799
M = 0.20	0	801	[a]802
	–3	804	805
	–4	806	807
	3	809	[a]810
	4	811	812
	8	813	[a]814
M = 0.22	0	817	[a]818
	–3	819	820
	–4	821	822
	3	824	825
	4	826	827
	8	828	829

[a]These readings can be used to correct virtually all the powered data

TABLE 14.—8- BY 6-ft SWT TARE READINGS

Plate height above model centerline, in.	Mach 0.27	Mach 0.45	Mach 0.60	Mach 0.67	Mach 0.73	Mach 0.75	Mach 0.78	Mach 0.80
45.7	530	548	567	585	603	624	642	660
39.58	531	550	568	586	604	625	643	661
38.76	532	551	569	587	605	626	644	662
36.14	533	552	570	588	606	627	645	663
34.4	534	553	571	589	607	628	646	664
31.32	535	554	572	590	608	629	647	665
30.67	536	555	573	591	609	630	648	666
28.58	537	556	574	592	613	631	649	667
27.21	538	557	575	593	614	632	650	668
23.04	539	558	576	594	615	633	651	669
22.57	540	559	577	595	616	634	652	670
21.03	541	560	578	596	617	635	653	671
20.02	542	561	579	597	618	636	654	672
18.91	543	562	580	598	619	637	655	673
18.52	544	563	581	599	620	638	656	674
17.25	545	564	582	600	621	639	657	675
16.79	546	565	583	601	622	640	658	676

TABLE 15.—EXPECTED SHAFT ORDER TONES FOR 12×10 OPEN ROTOR

	n = 0	n = 1	n = 2	n = 3	n = 4	n = 5	n = 6
m = 0		10	20	30	40	50	60
m = 1	12	22	32	42	52	62	72
m = 2	24	34	44	54	64	74	84
m = 3	36	46	56	66	76	86	96
m = 4	48	58	68	78	88	98	108
m = 5	60	70	80	90	100	110	120
m = 6	72	82	92	102	112	122	132

Figure 1.—F31/A31 rotor blades, shown with a 1 ft ruler for scale.

Figure 2.—ORPR in 9- by 15-ft LSWT.

Figure 3.—ORPR installed in 8- by 6-ft SWT with Kulite plate above.

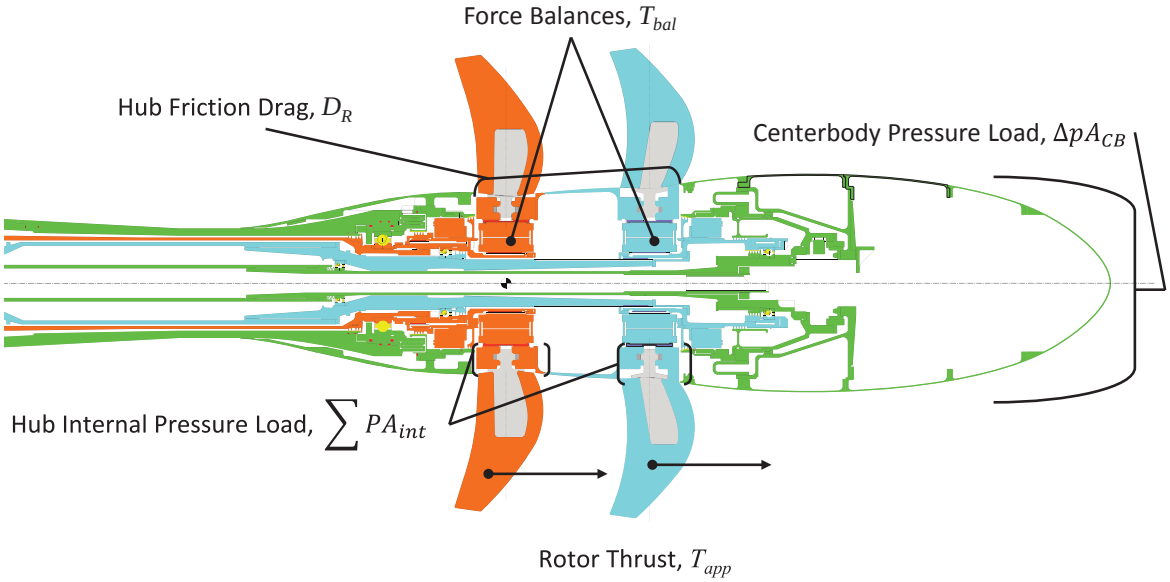

Figure 4.—Force diagram for ORPR performance calculations.

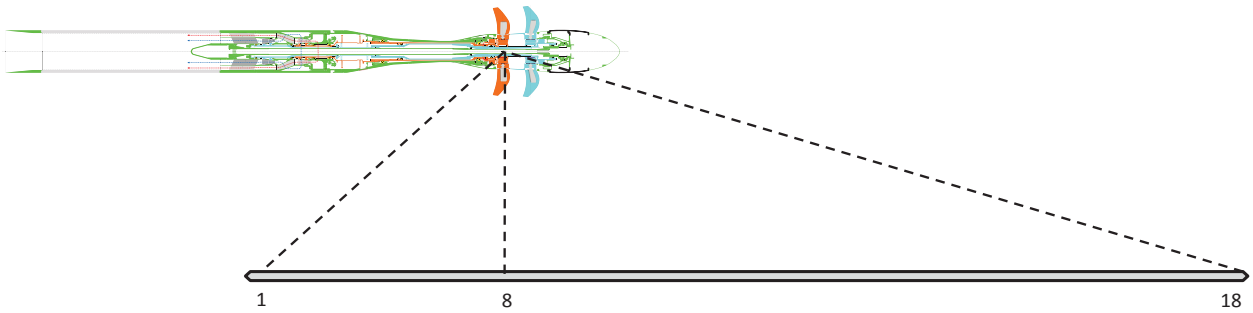

Figure 5.—Diagram of microphone locations in the 9- by 15-ft LSWT. Scale is approximate.

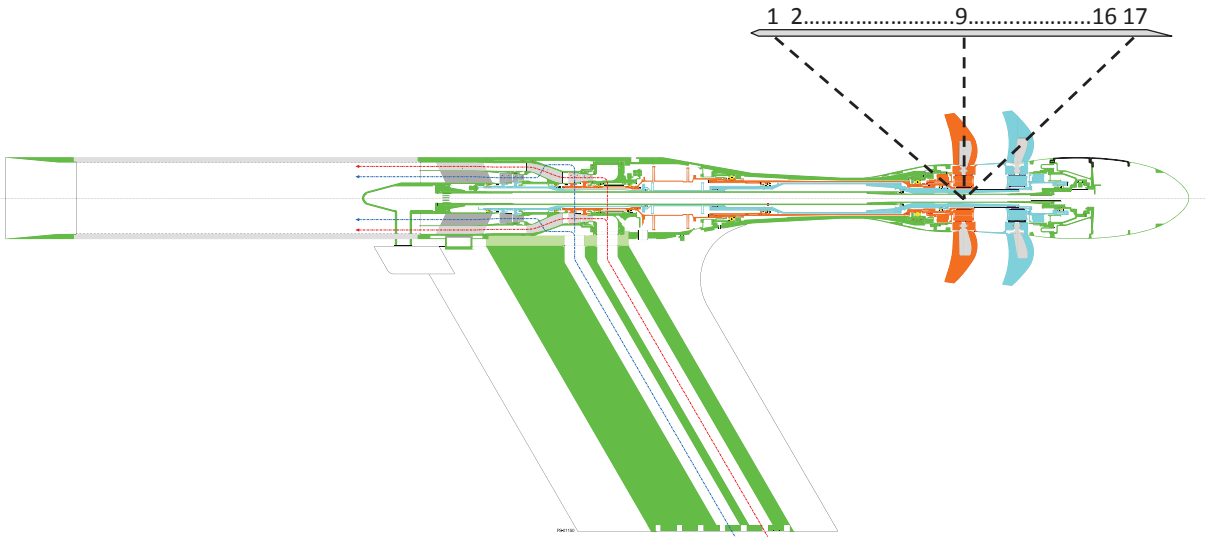

Figure 6.—Nearfield pressure instrumentation for ORPR 8- by 6-ft SWT test. Scale is approximate.

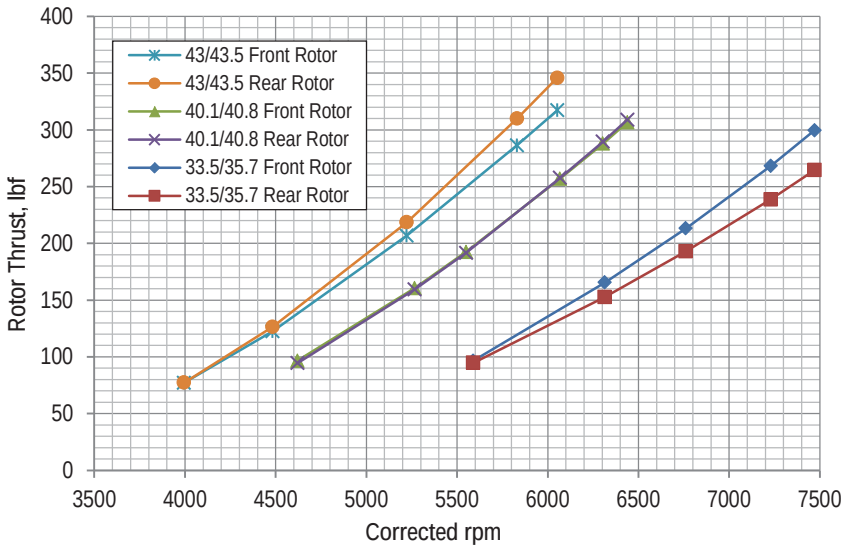

Figure 7.—Rotor thrust, M = 0.20.

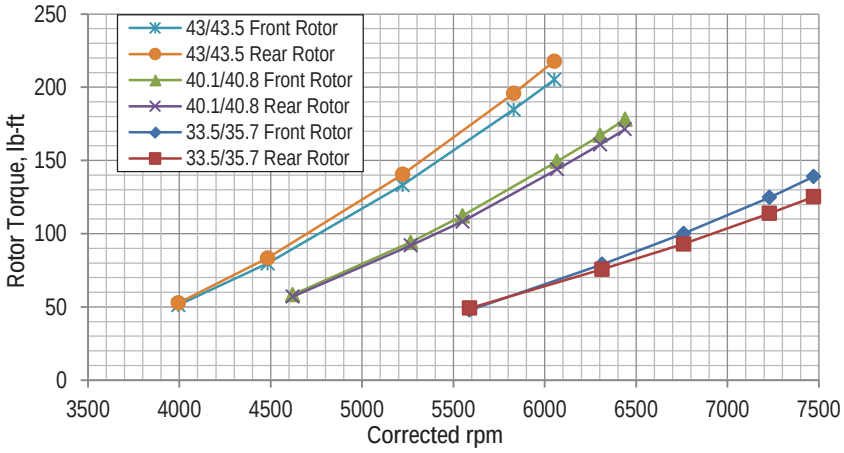

Figure 8.—Rotor torque, M = 0.20.

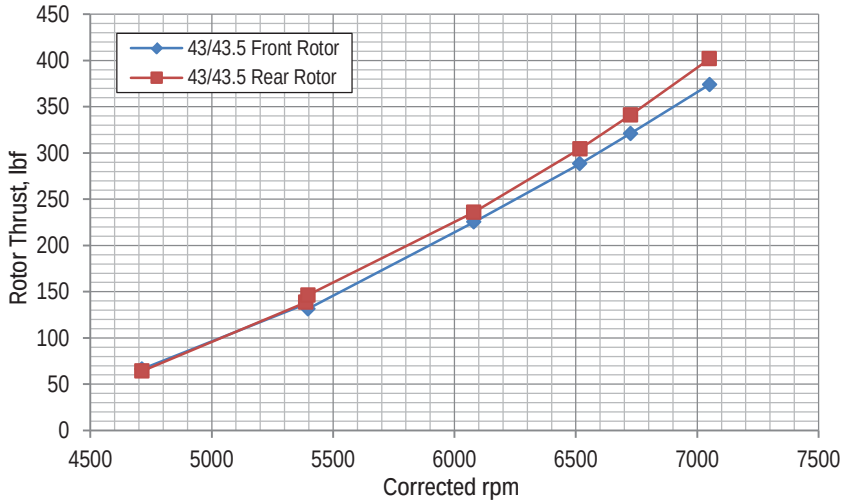

Figure 9.—Rotor thrust, M = 0.27.

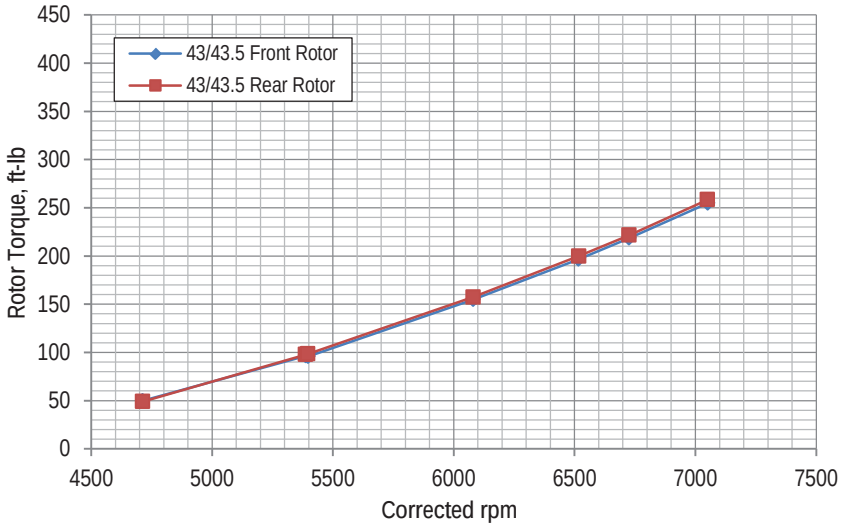

Figure 10.—Rotor torque, M = 0.27.

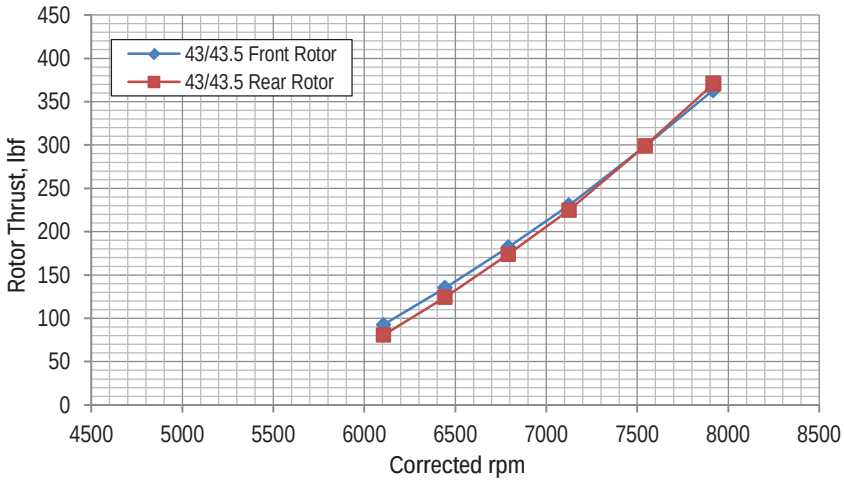

Figure 11.—Rotor thrust, M = 0.36.

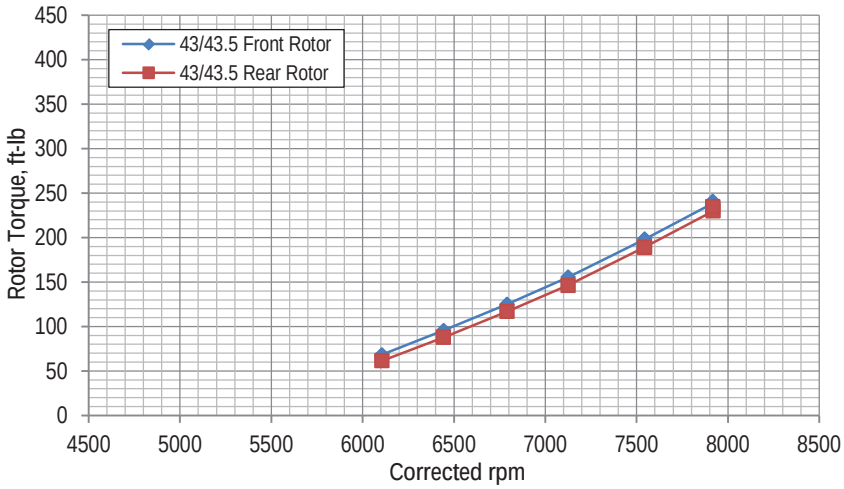

Figure 12.—Rotor torque, M = 0.36.

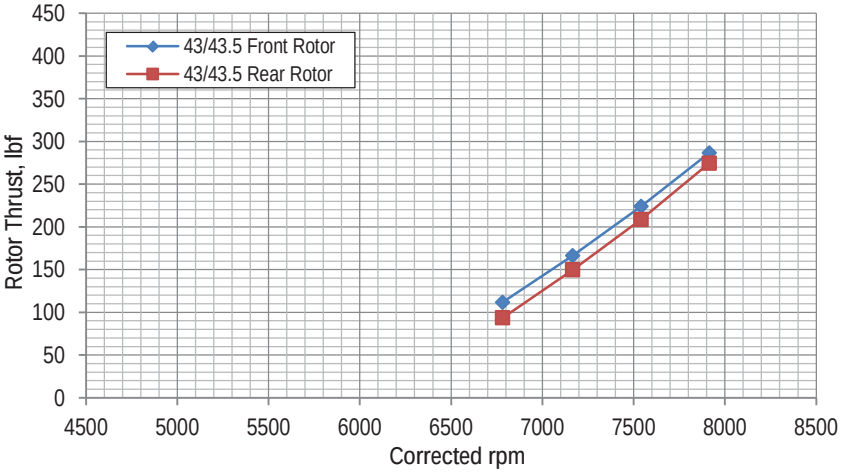

Figure 13.—Rotor thrust, M = 0.40.

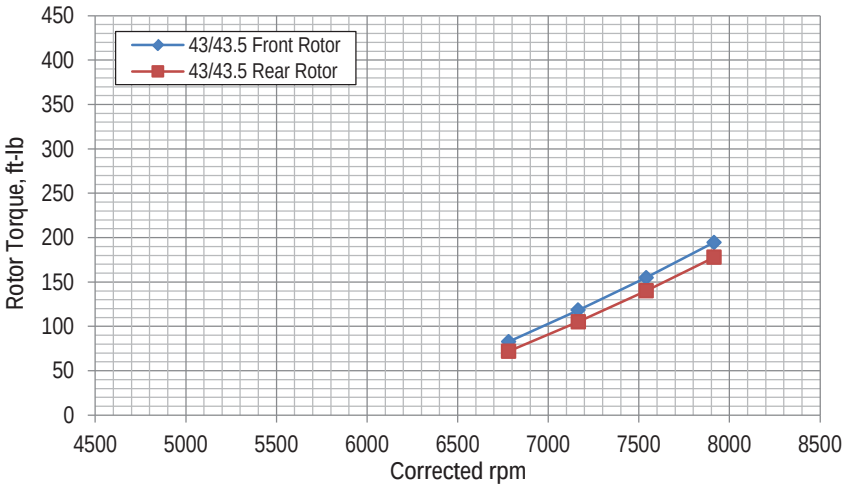

Figure 14.—Rotor torque, M = 0.40.

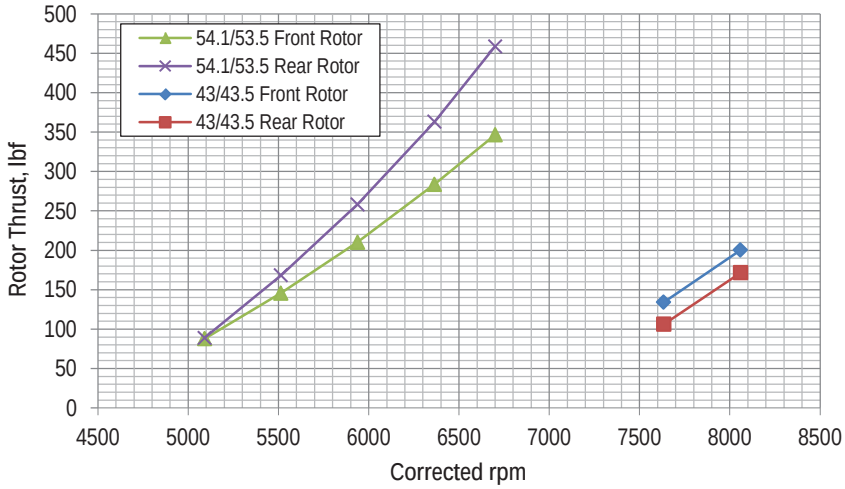

Figure 15.—Rotor thrust, M = 0.45.

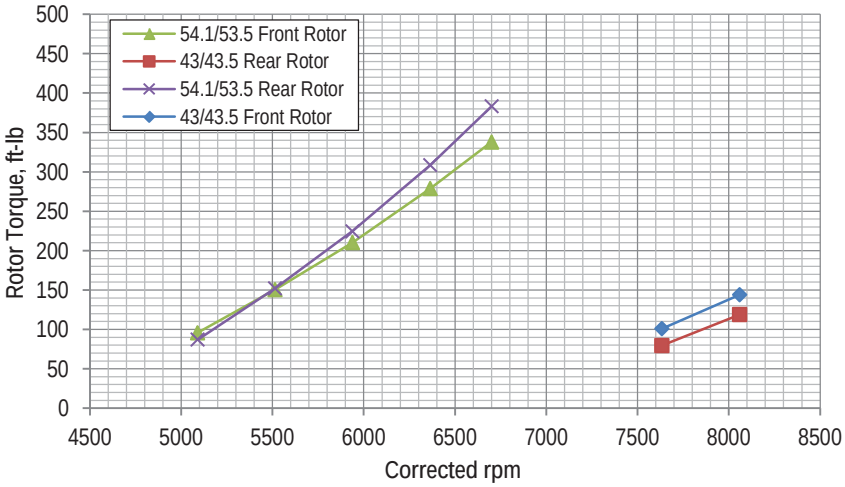

Figure 16.—Rotor Torque, M = 0.45.

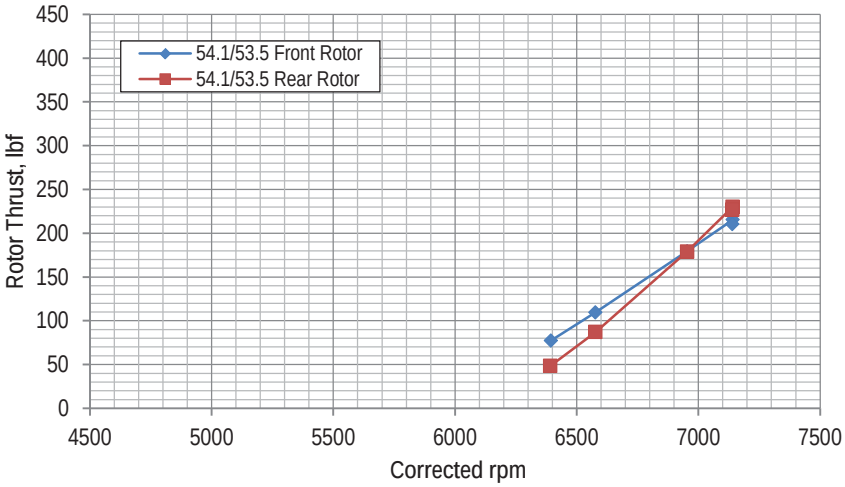

Figure 17.—Rotor thrust, M = 0.60.

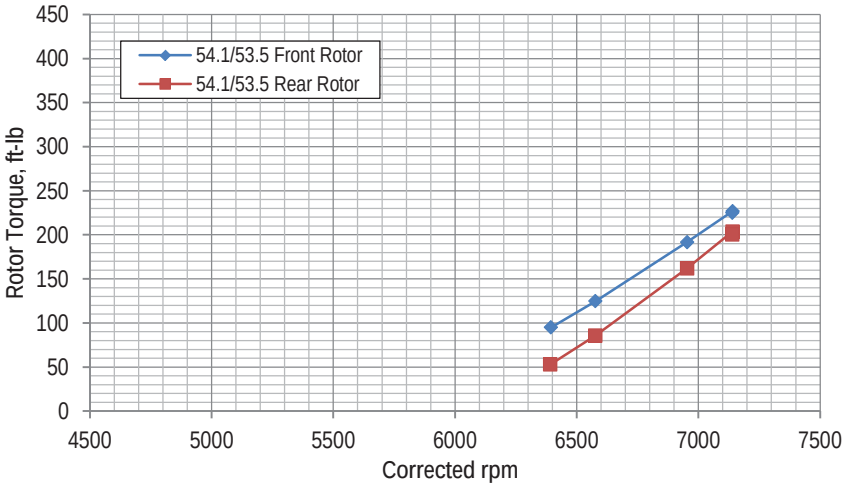

Figure 18.—Rotor torque, M = 0.60.

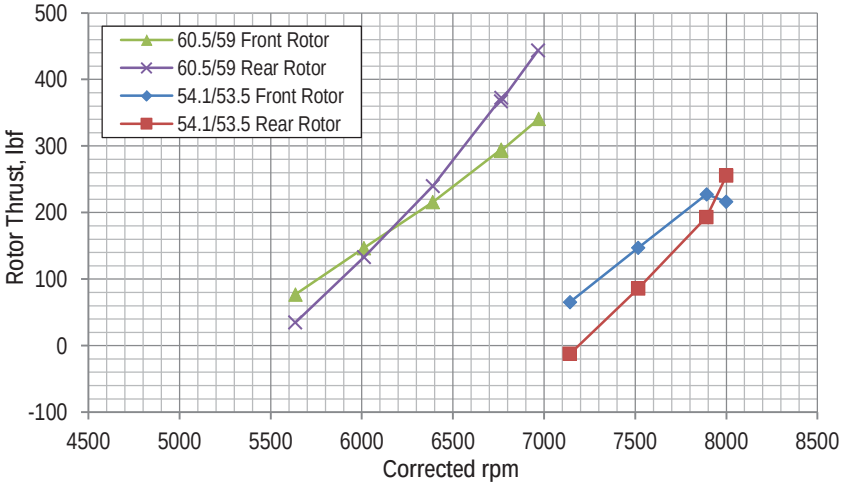

Figure 19.—Rotor thrust, M = 0.67.

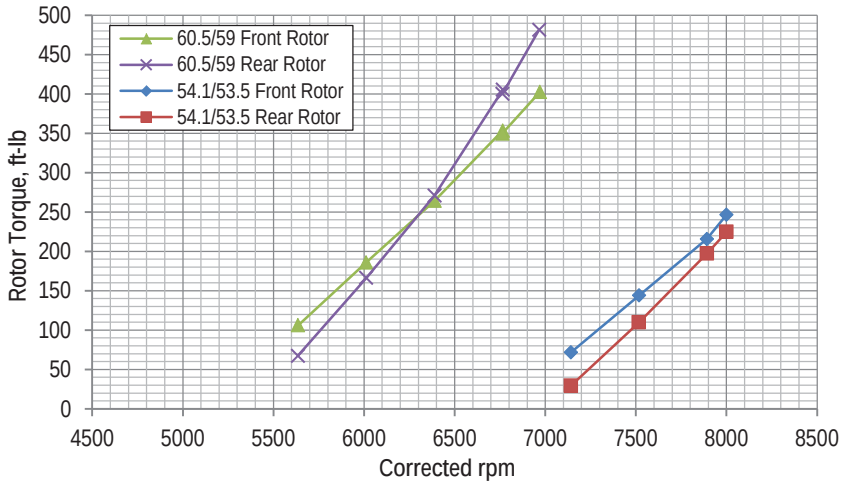

Figure 20.—Rotor torque, M = 0.67.

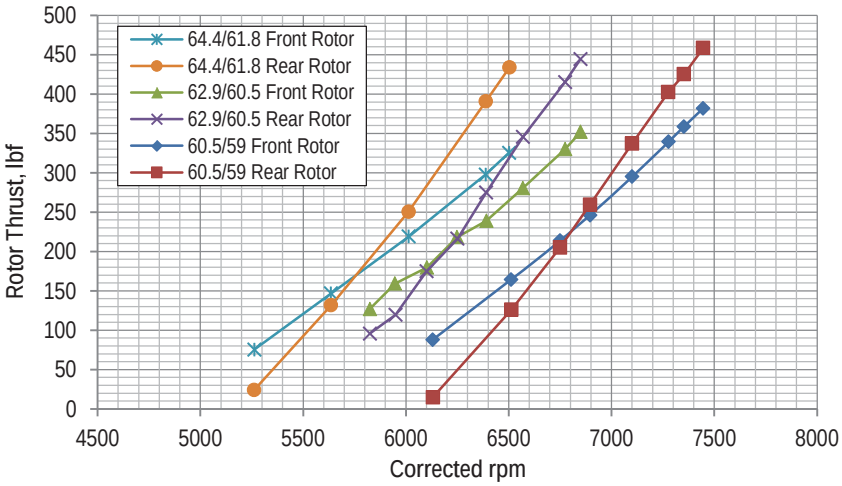

Figure 21.—Rotor thrust, M = 0.73.

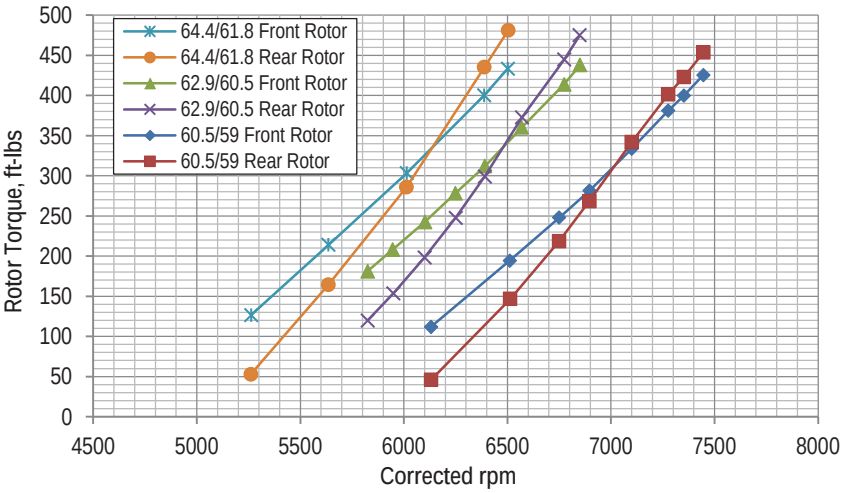

Figure 22.—Rotor torque, M = 0.73.

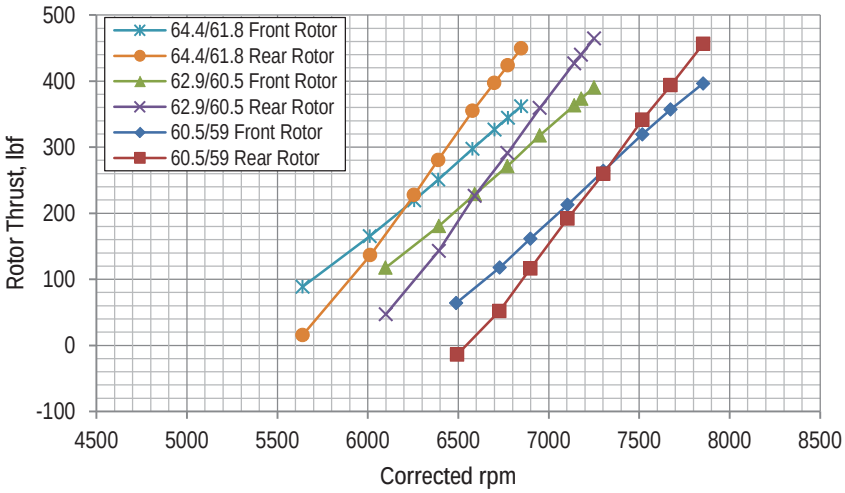

Figure 23.—Rotor thrust, M = 0.78.

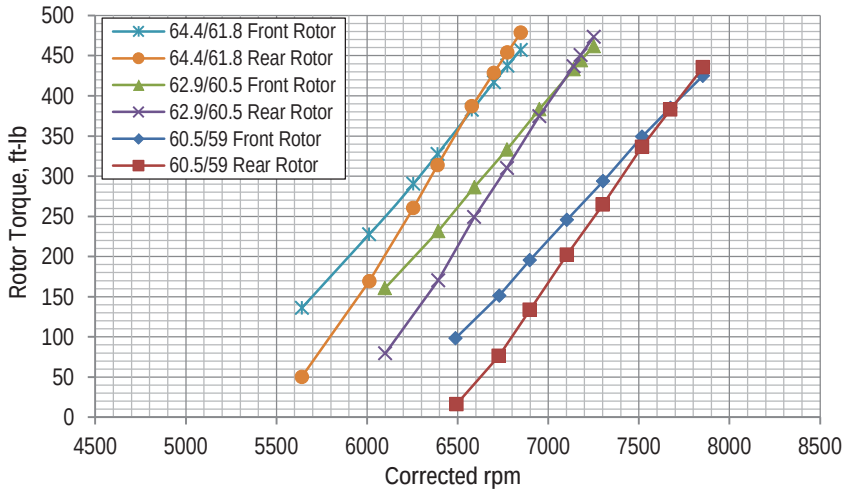

Figure 24.—Rotor torque, M = 0.78.

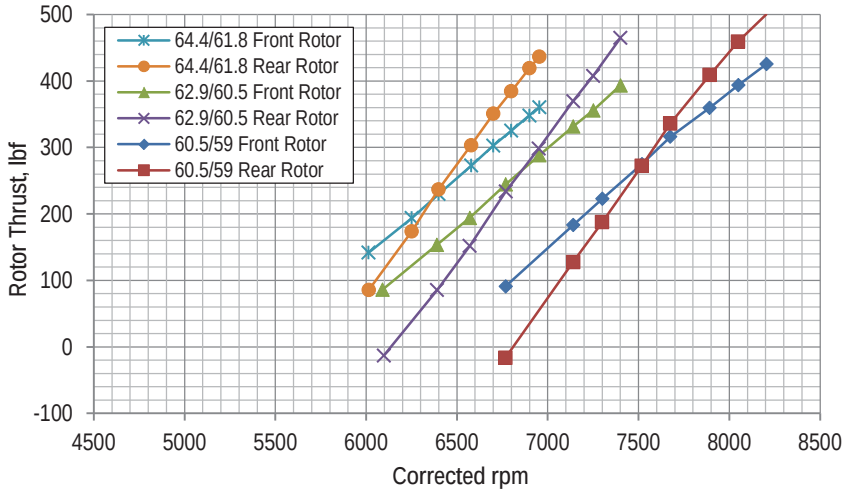

Figure 25.—Rotor thrust, M = 0.80.

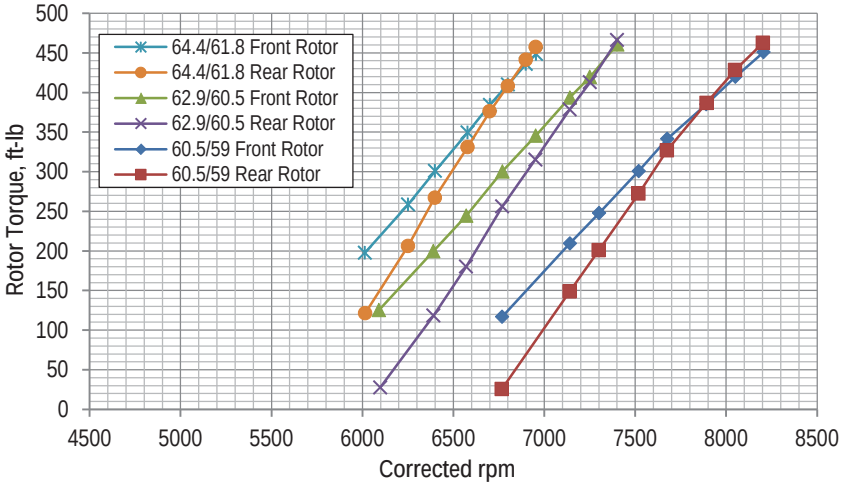

Figure 26.—Rotor torque, M = 0.80.

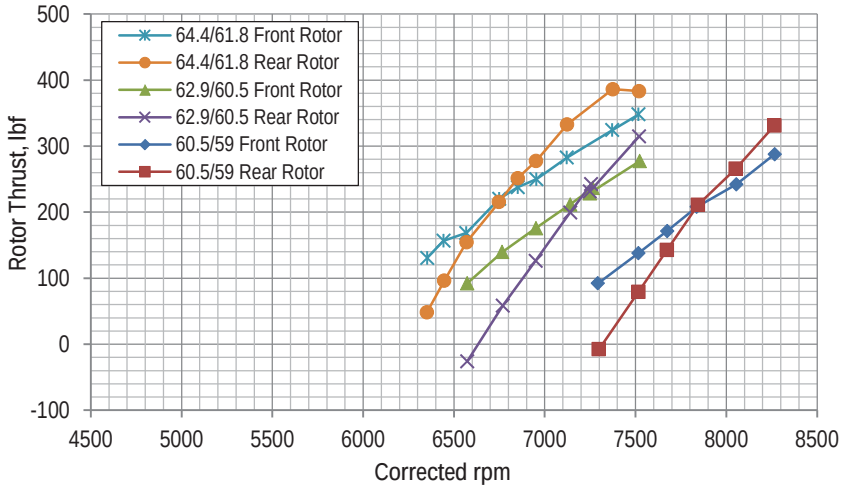

Figure 27.—Rotor thrust, M = 0.85.

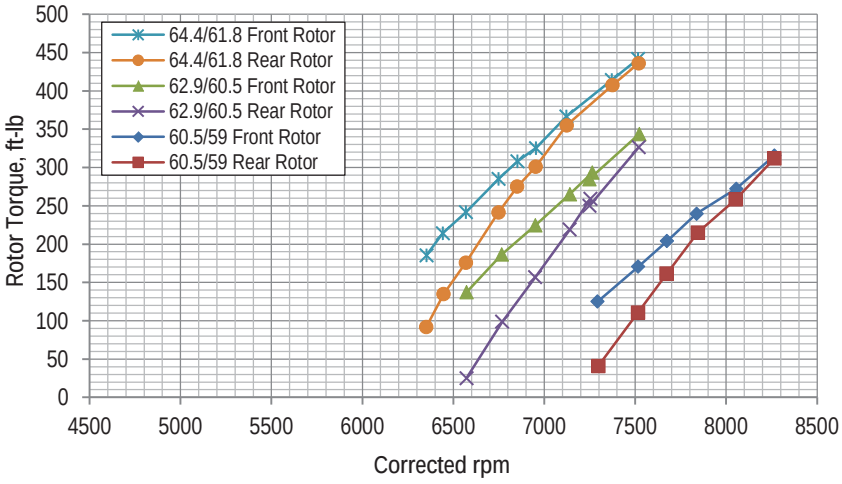

Figure 28.—Rotor thrust, M = 0.85.

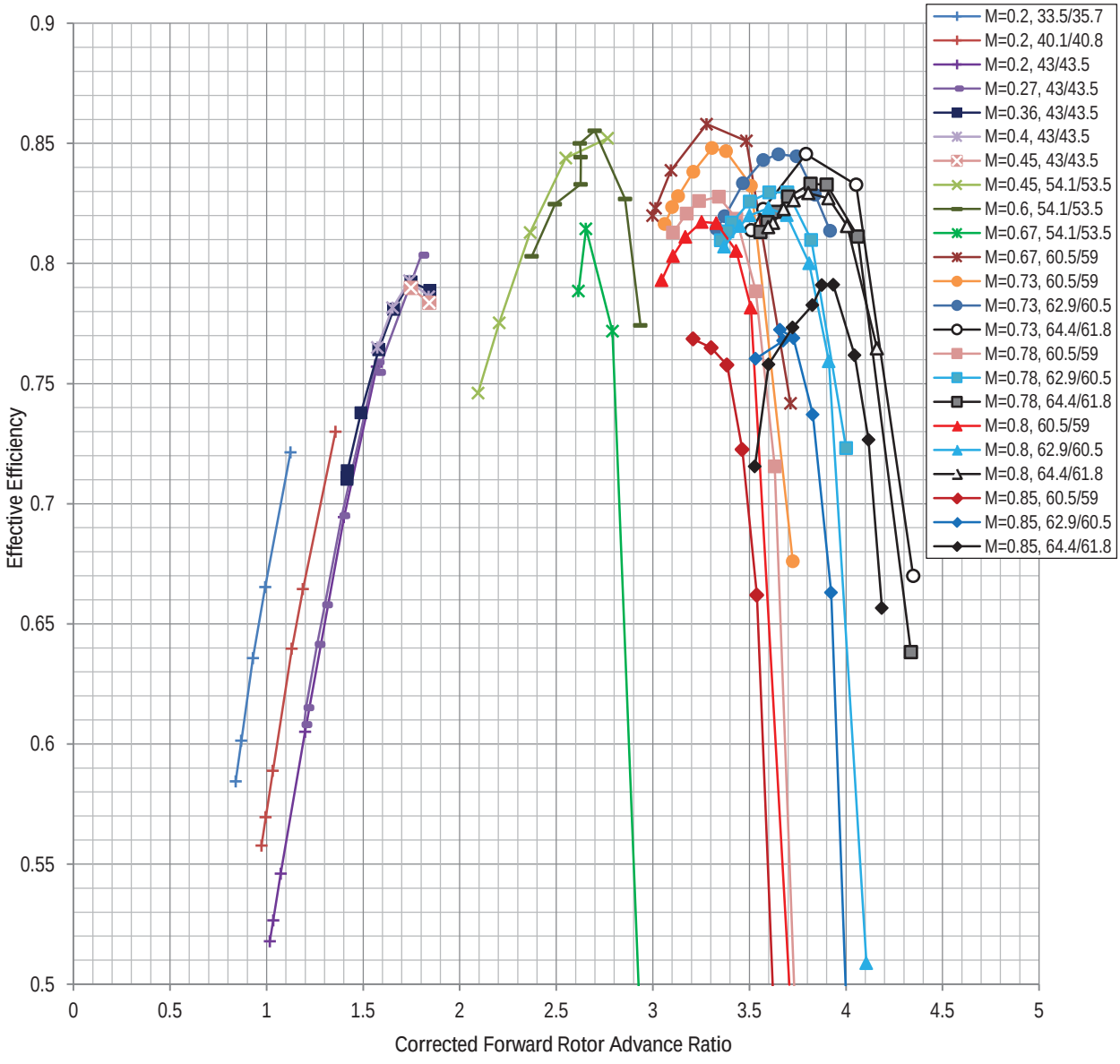

Figure 29.—Effective efficiency versus forward rotor advance ratio.

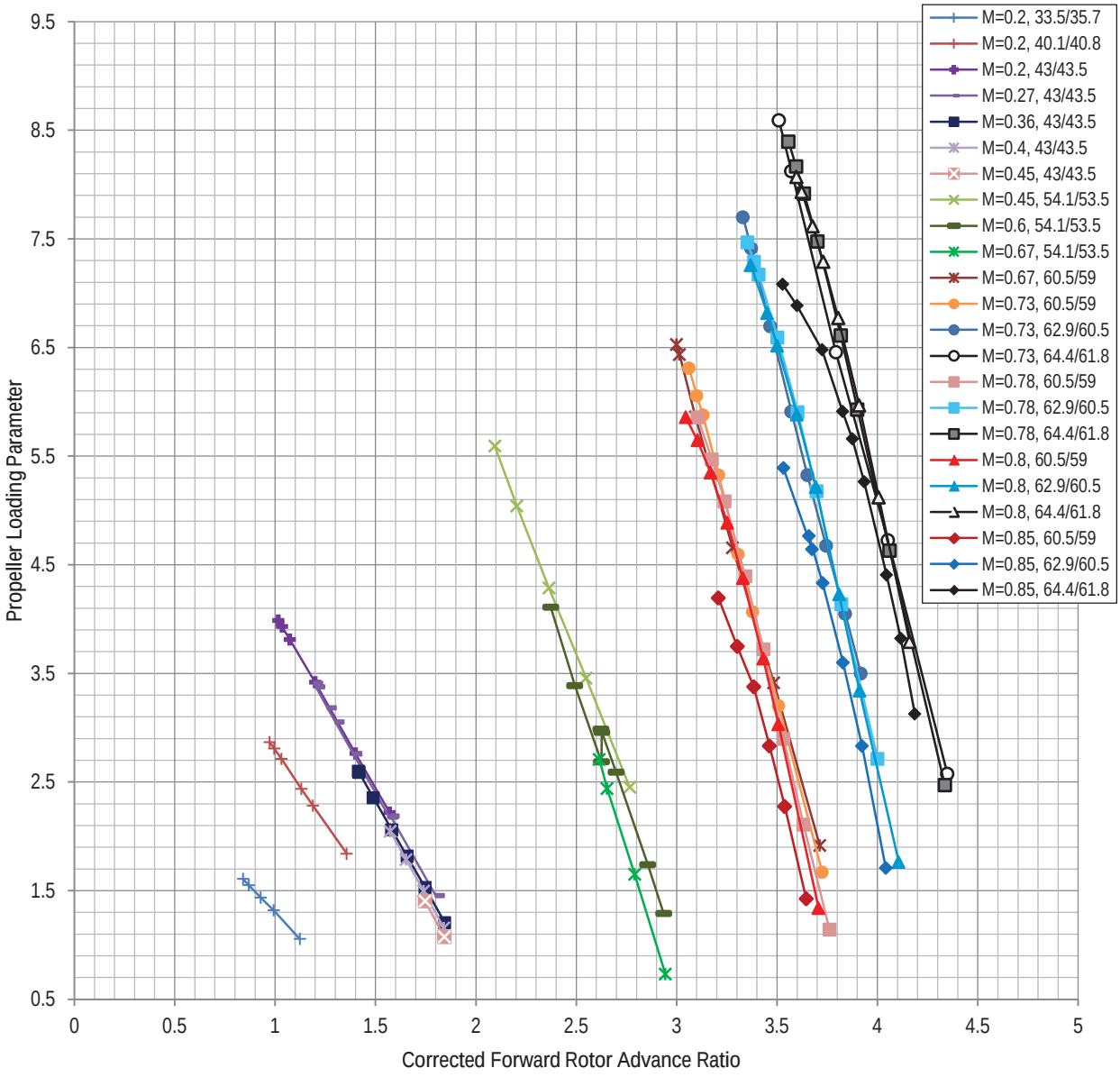

Figure 30.—Propeller loading parameter versus advance ratio.

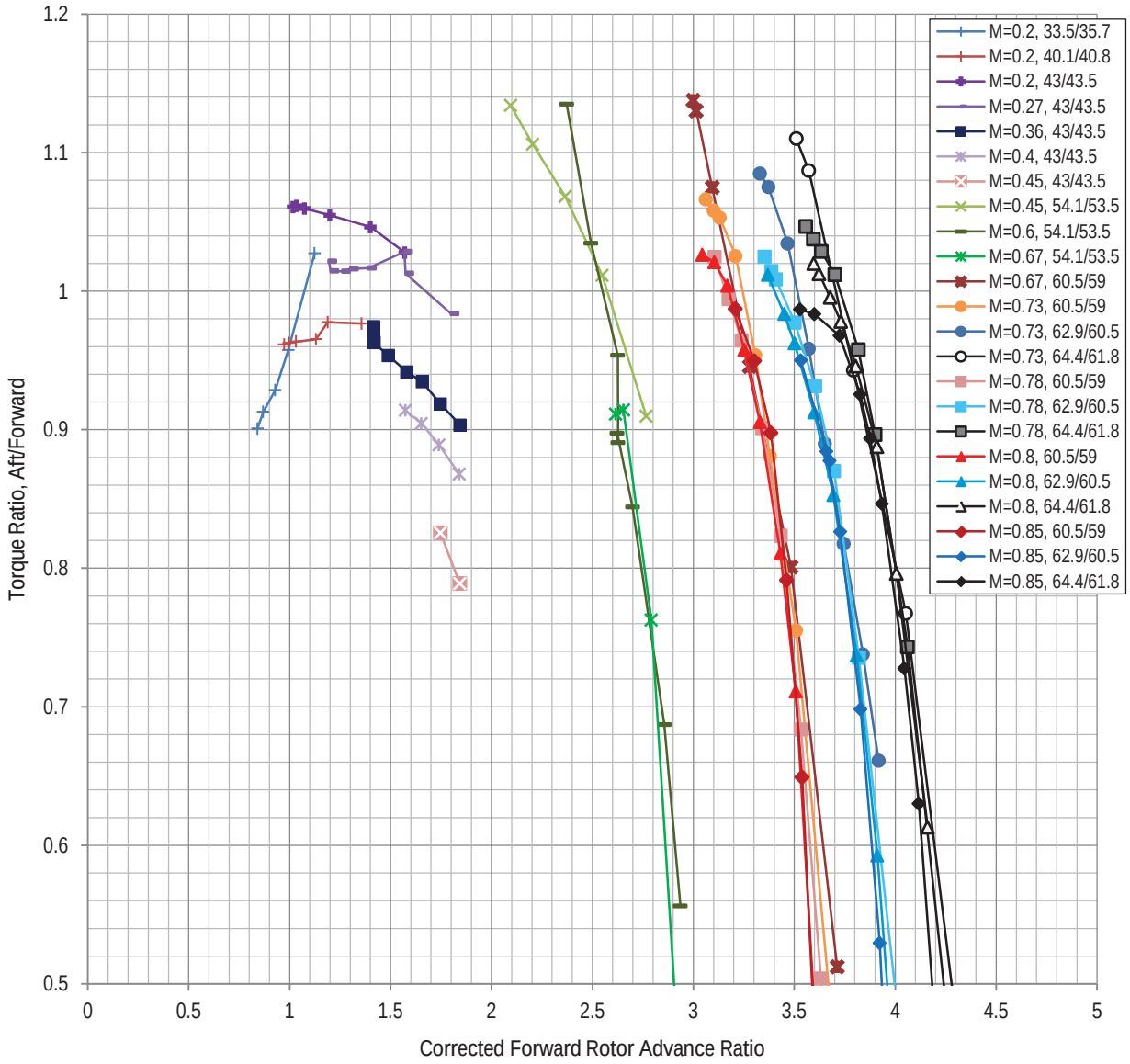

Figure 31.—Torque ratio versus advance ratio.

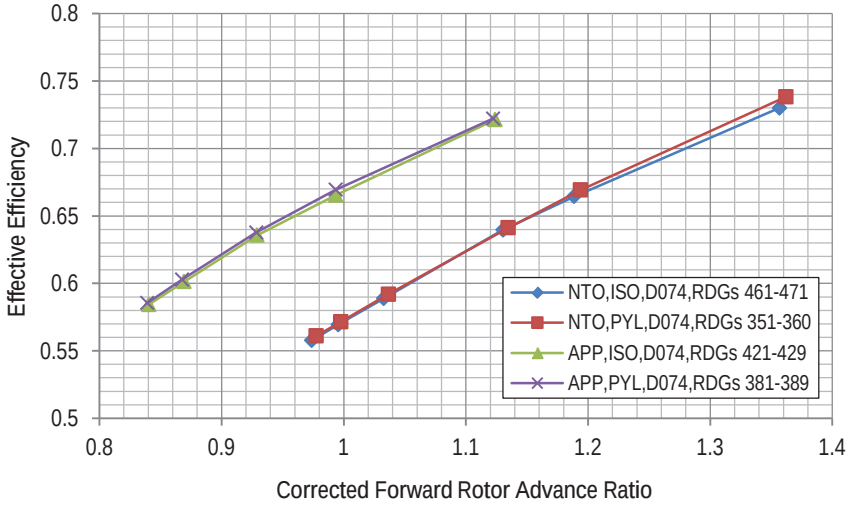

Figure 32.—Effect of pylon on efficiency at AoA = 0, M = 0.20.

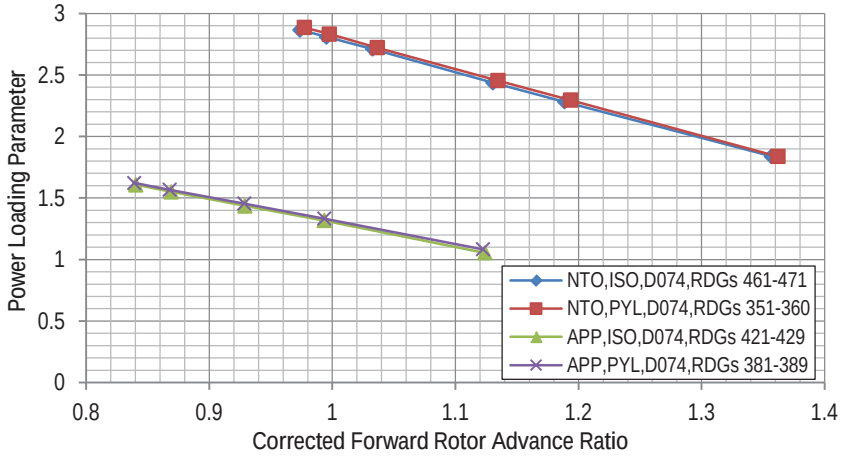

Figure 33.—Effect of pylon on propeller loading at AoA = 0, M = 0.20.

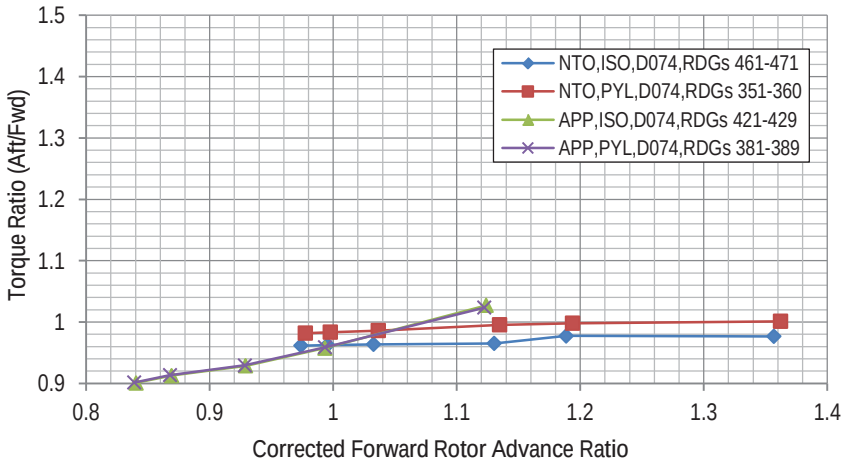

Figure 34.—Effect of pylon on torque ratio at AoA = 0, M = 0.20.

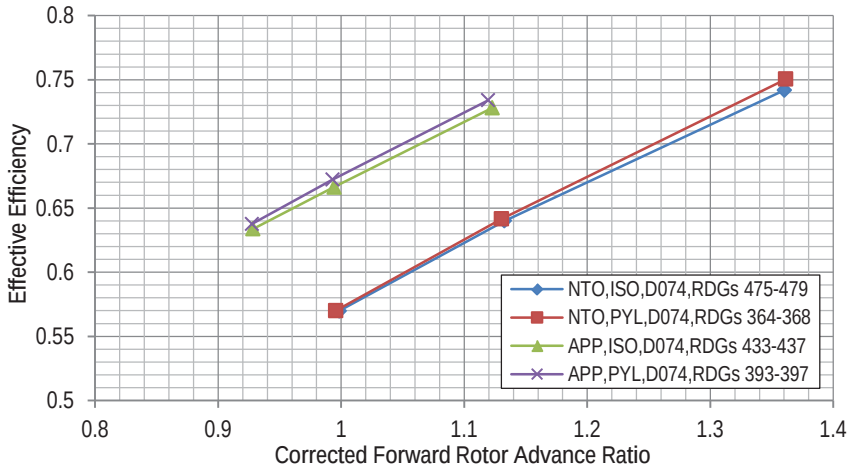

Figure 35.—Effect of pylon on efficiency at AoA = 3, M = 0.20.

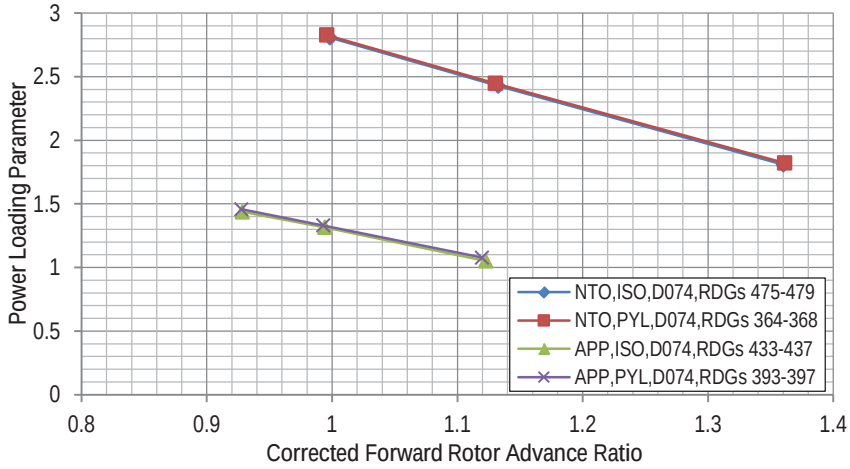

Figure 36.—Effect of pylon on propeller loading at AoA = 3, M = 0.20.

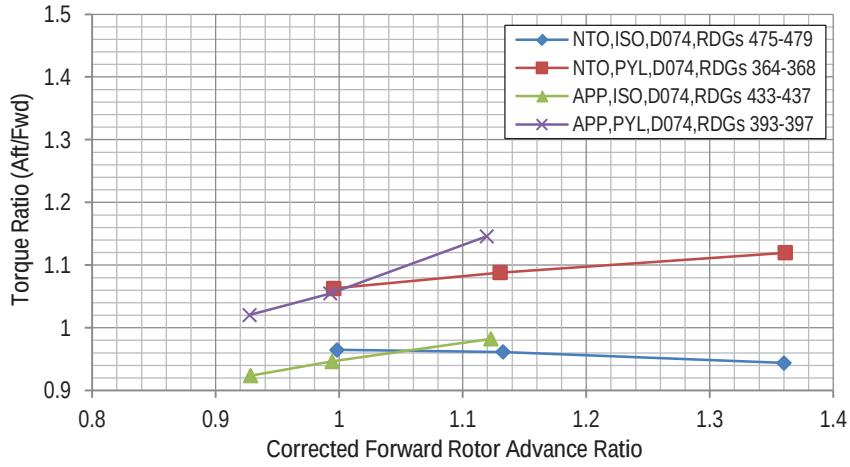

Figure 37.—Effect of pylon on torque ratio at AoA = 3, M = 0.20.

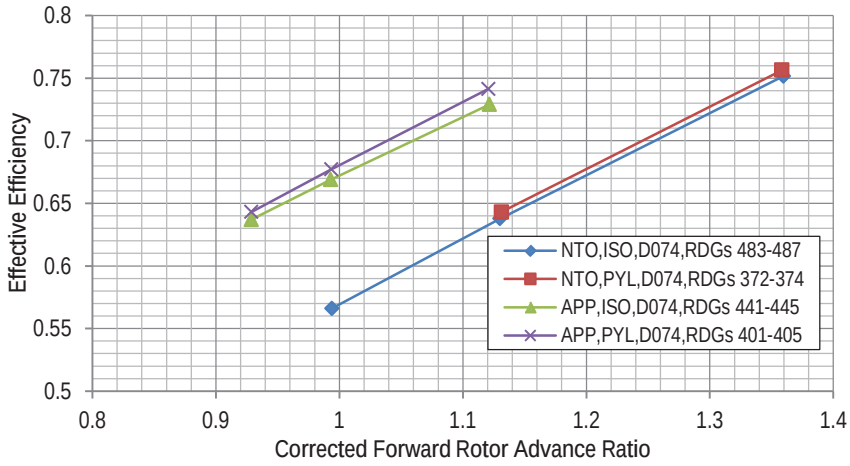

Figure 38.—Effect of pylon on efficiency at AoA = 8, M = 0.20.

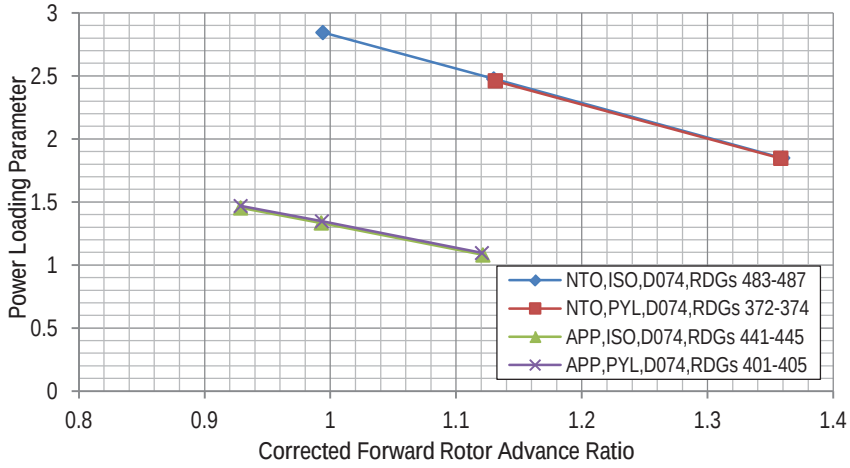

Figure 39.—Effect of pylon on propeller loading at AoA = 8, M = 0.20.

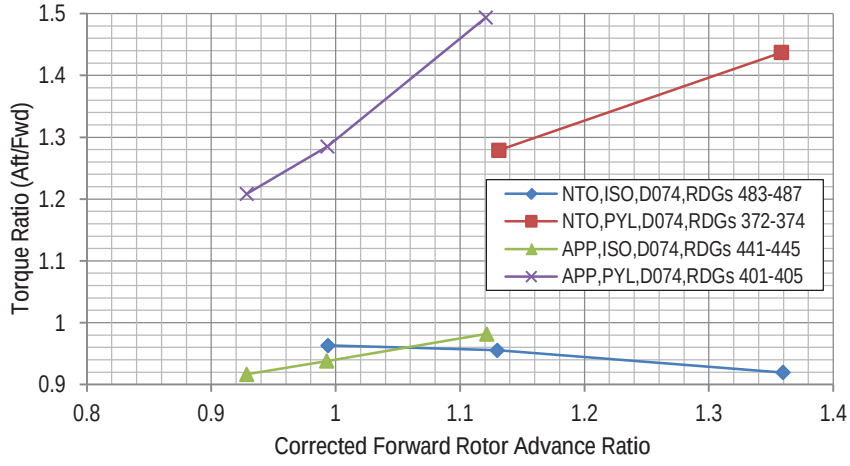

Figure 40.—Effect of pylon on torque ratio at AoA = 8, M = 0.20.

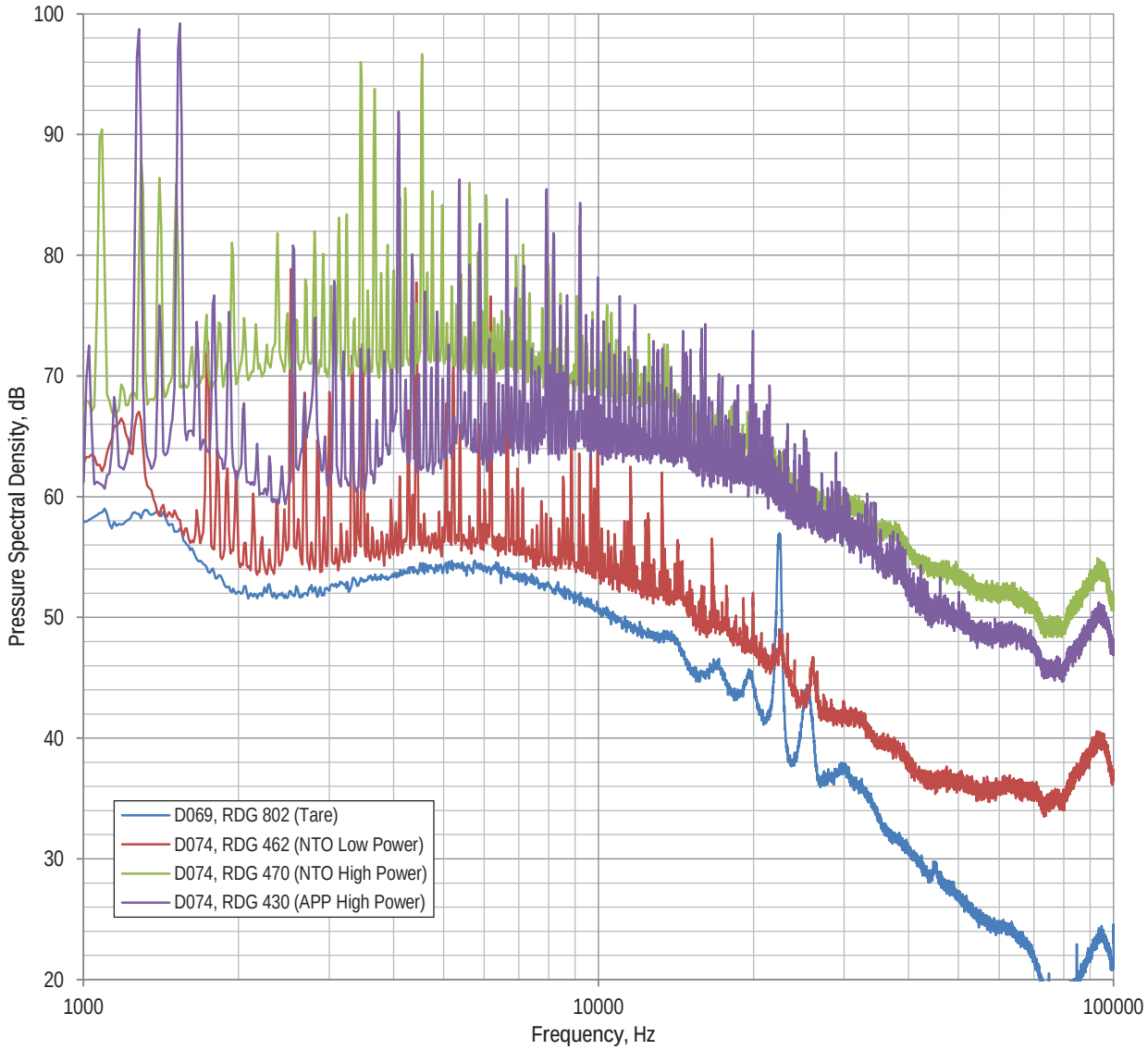

Figure 41.—Sample spectra from 9- by 15-ft LSWT.

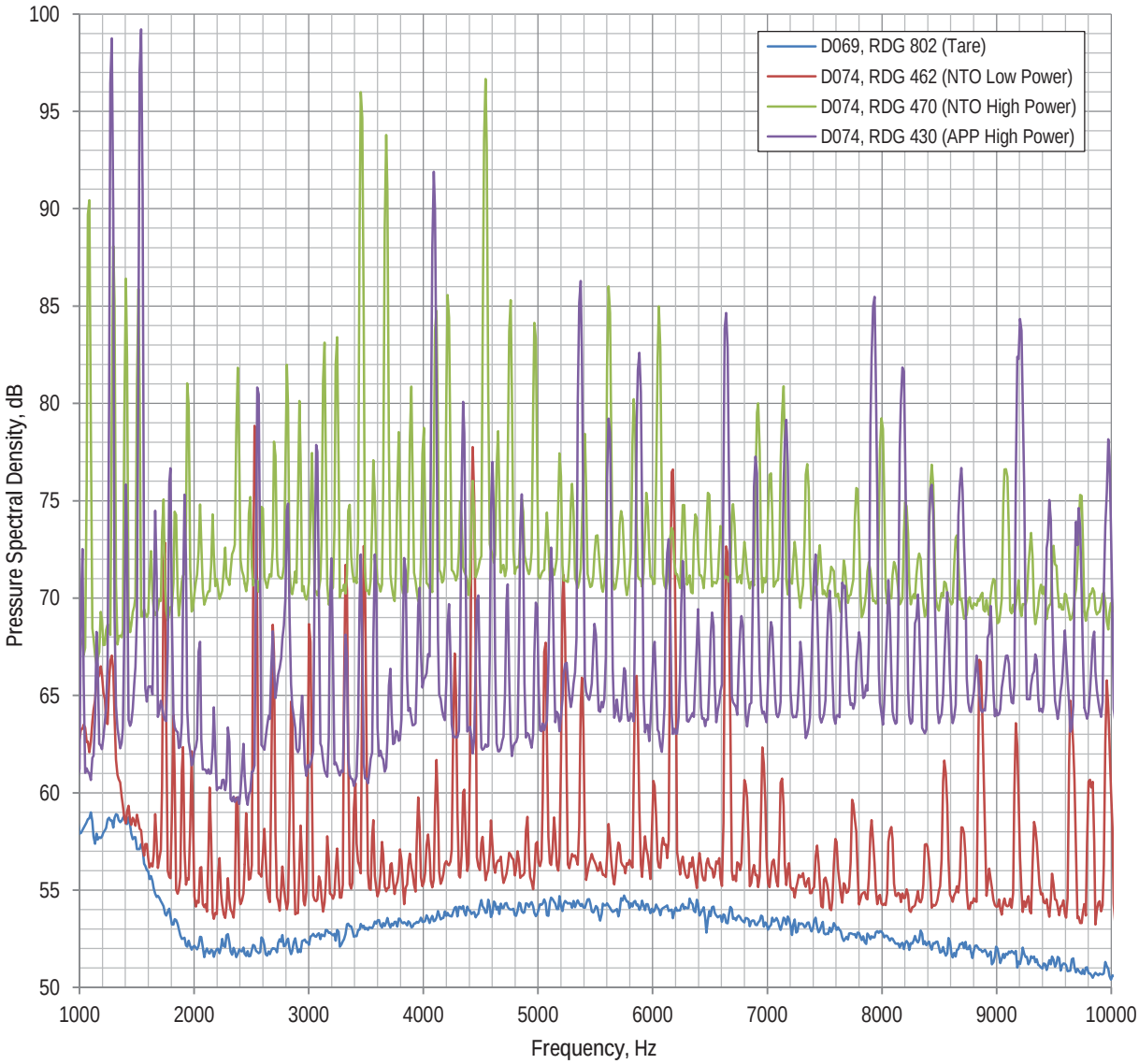

Figure 42.—Sample spectra from 9- by 15-ft LSWT (zoom).

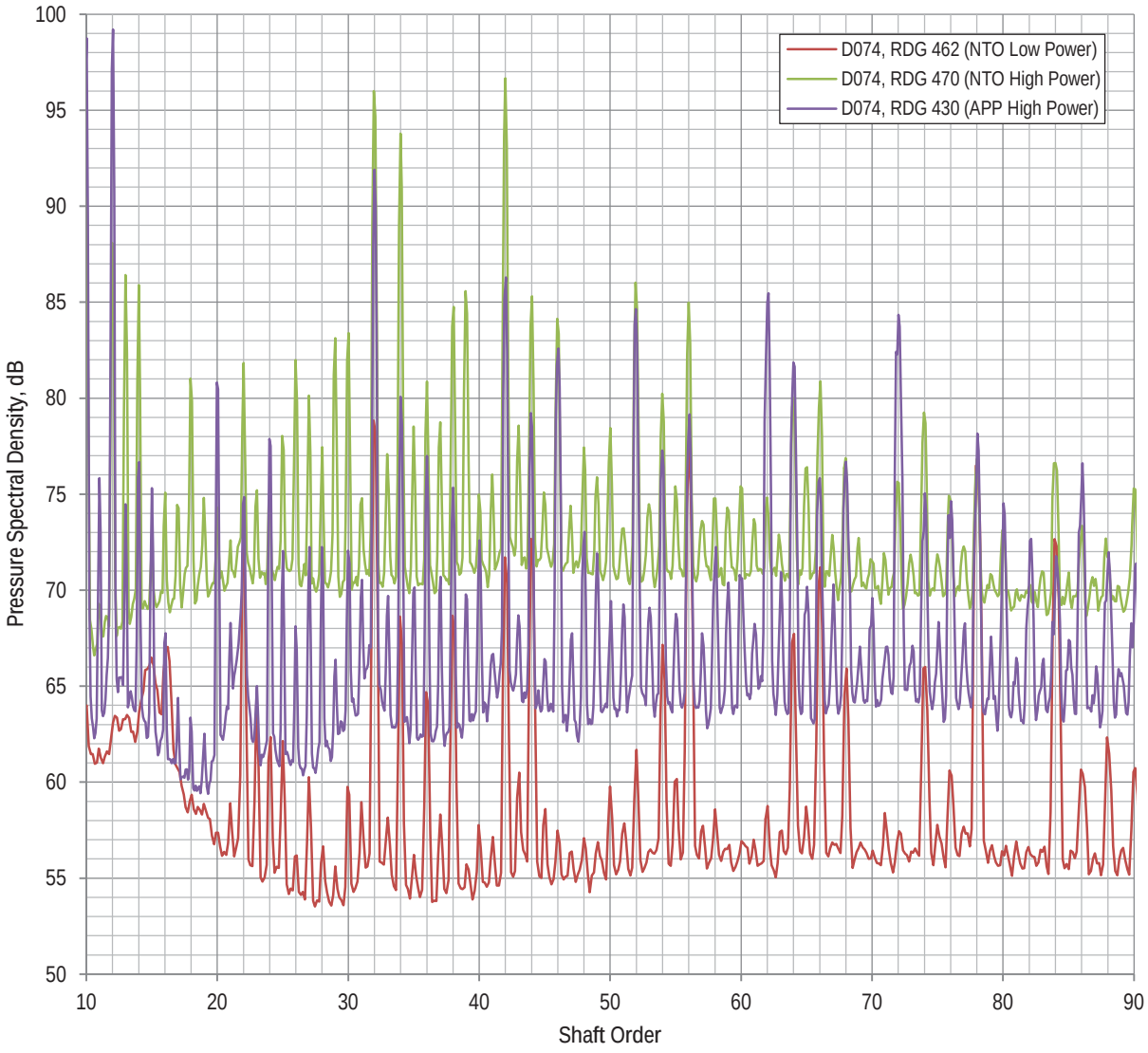

Figure 43.—Sample spectra from 9- by 15-ft LSWT shown in terms of shaft order.

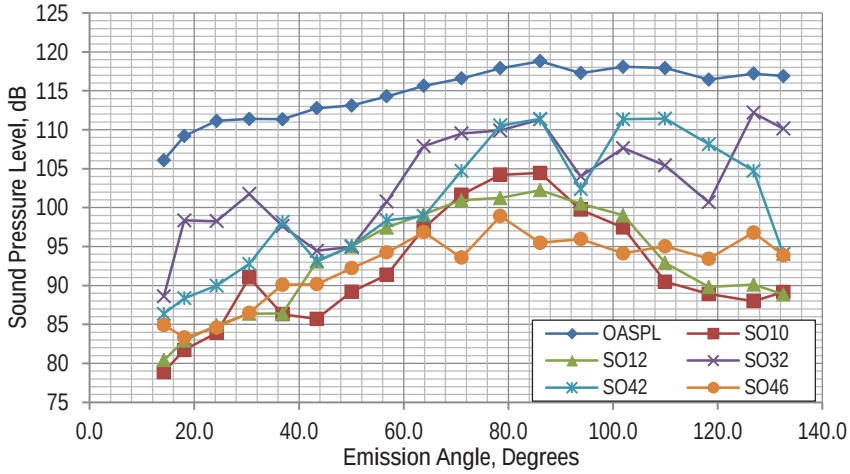

Figure 44.—Tone directivity, nominal take-off, isolated, M = 0.20, 578 lbf thrust, D074 RDG 470.

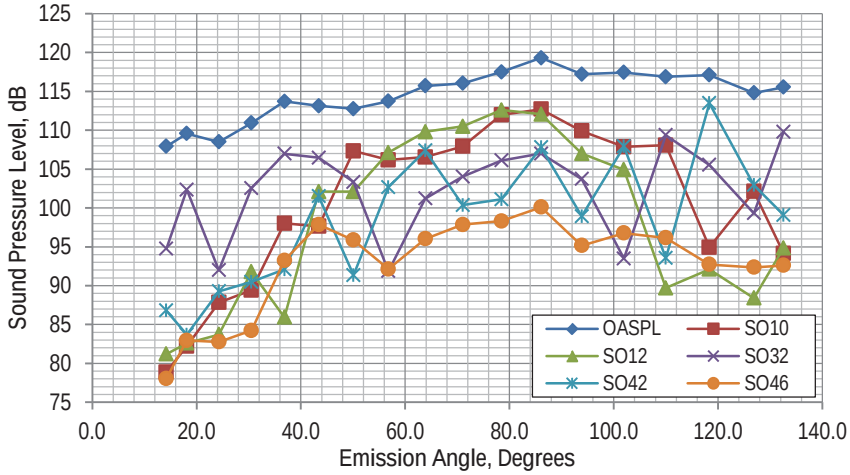

Figure 45.—Tone directivity, approach, isolated, M = 0.20, 564 lbf thrust, D074 RDG 430.

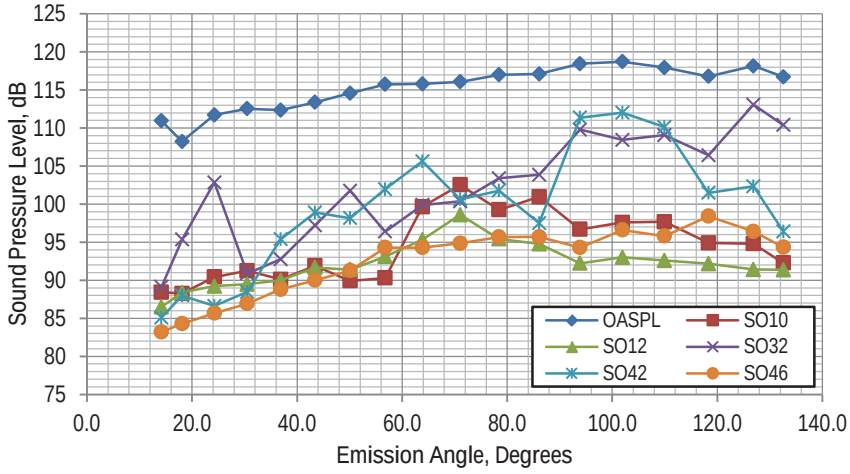

Figure 46.—Tone directivity, scaled take-off, isolated, AoA = 0, M = 0.20, 596 lbf thrust, D071 RDG 4286.

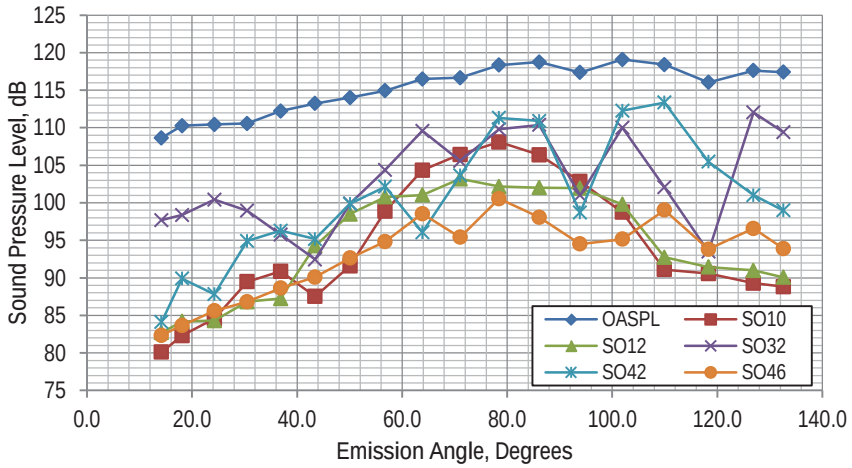

Figure 47.—Tone directivity, nominal take-off, isolated, AoA = 3, M = 0.20, 575 lbf thrust, D074 RDG 480.

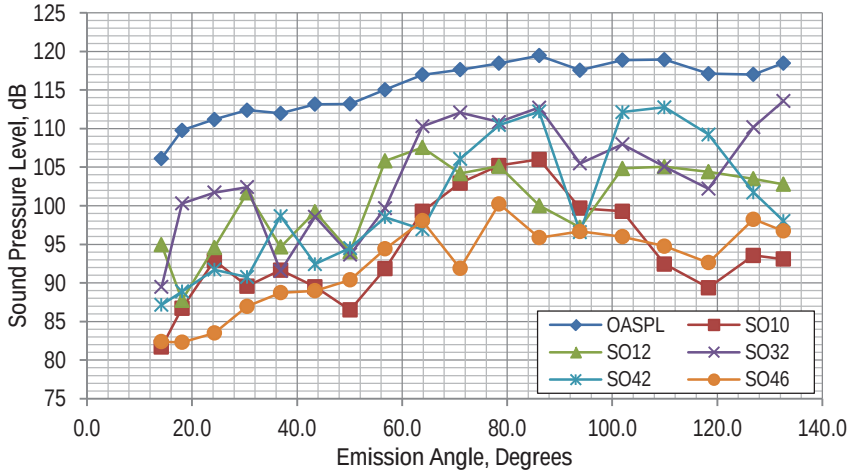

Figure 48.—Tone directivity, nominal take-off, pylon, AoA = 0, M = 0.20, 583 lbf thrust, D074 RDG 359.

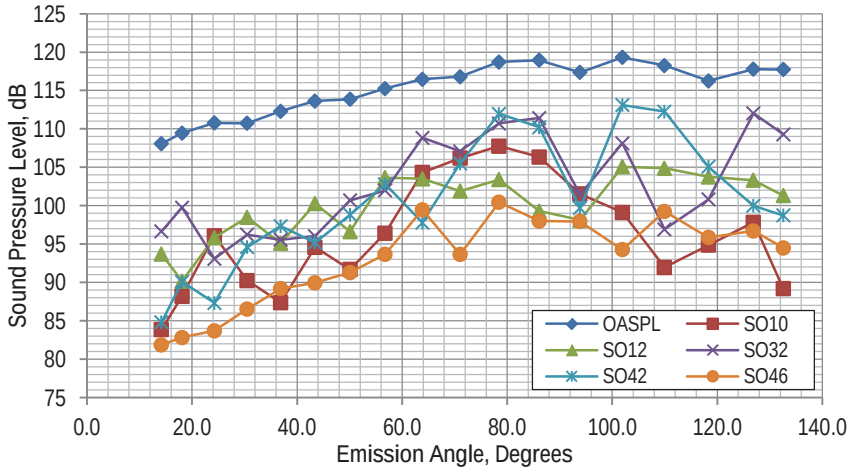

Figure 49.—Tone directivity, nominal take-off, pylon, AoA = 3, M = 0.20, 582 lbf thrust, D074 RDG 369.

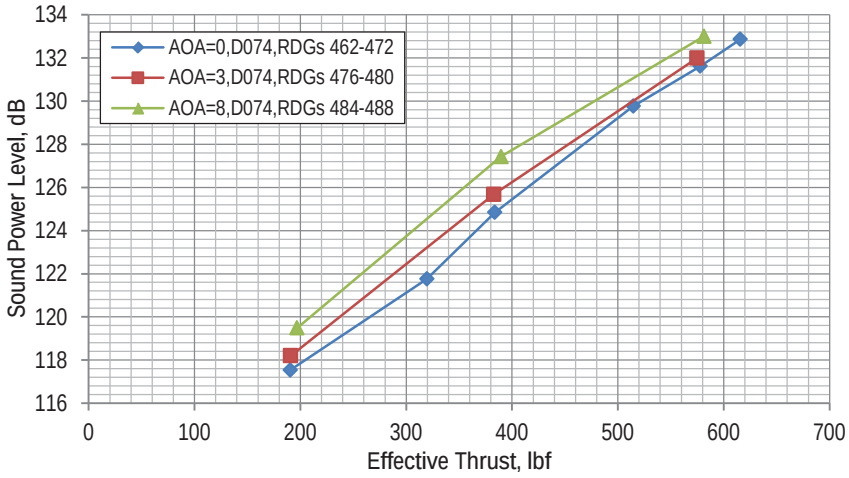

Figure 50.—Sound power level, nominal take-off, isolated, M = 0.20.

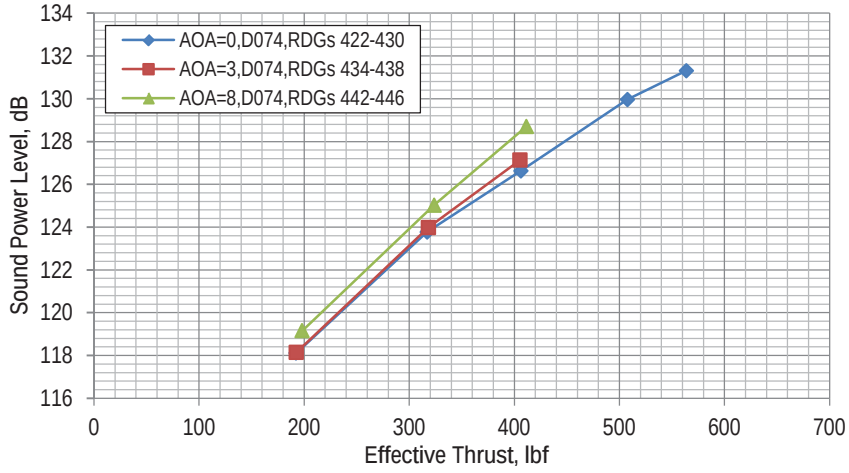

Figure 51.—Sound power level, approach, isolated, M = 0.20. (Blade stress levels limited data acquisition at AoA.)

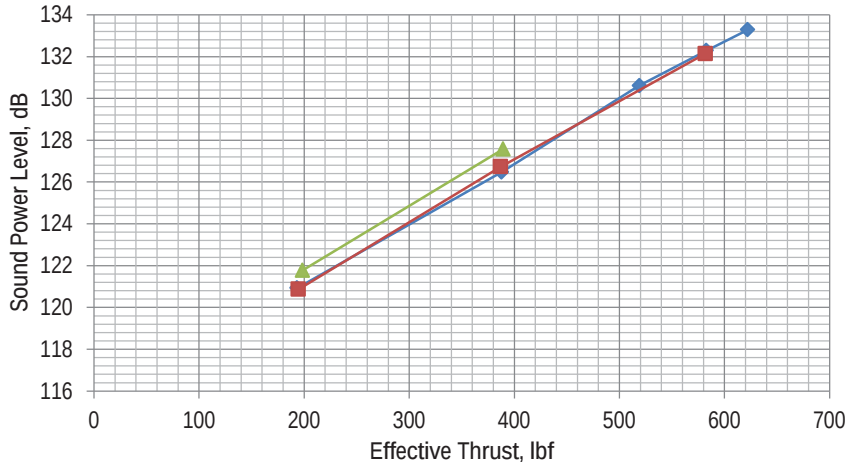

Figure 52.—Sound power level, nominal take-off, pylon, M = 0.20.

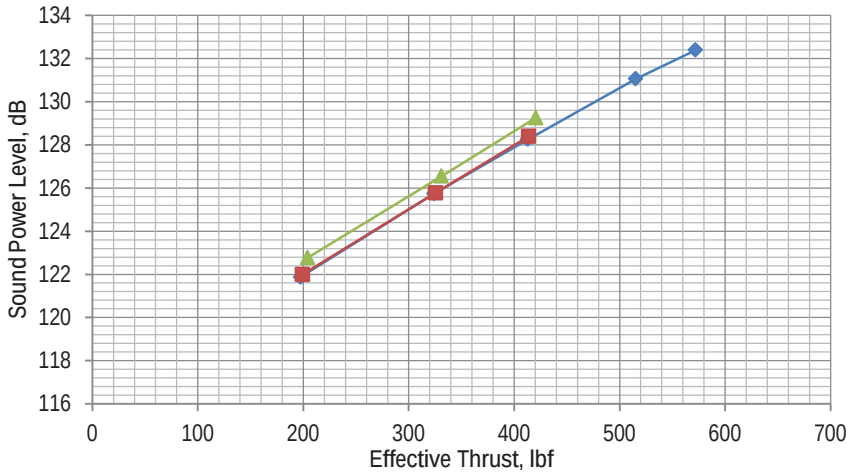

Figure 53.—Sound power level, approach, pylon, M = 0.20. (Blade stress levels limited data acquisition at AoA.)

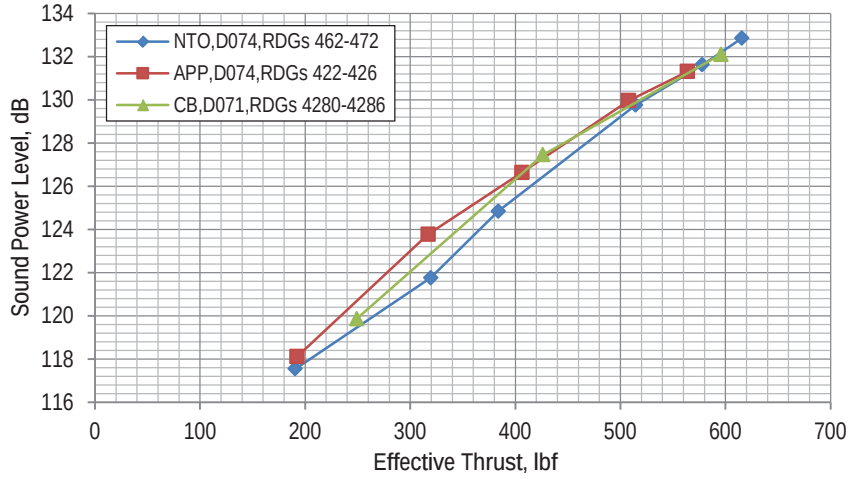

Figure 54.—Sound power level, isolated rotor comparing three pitch angles, M = 0.20.

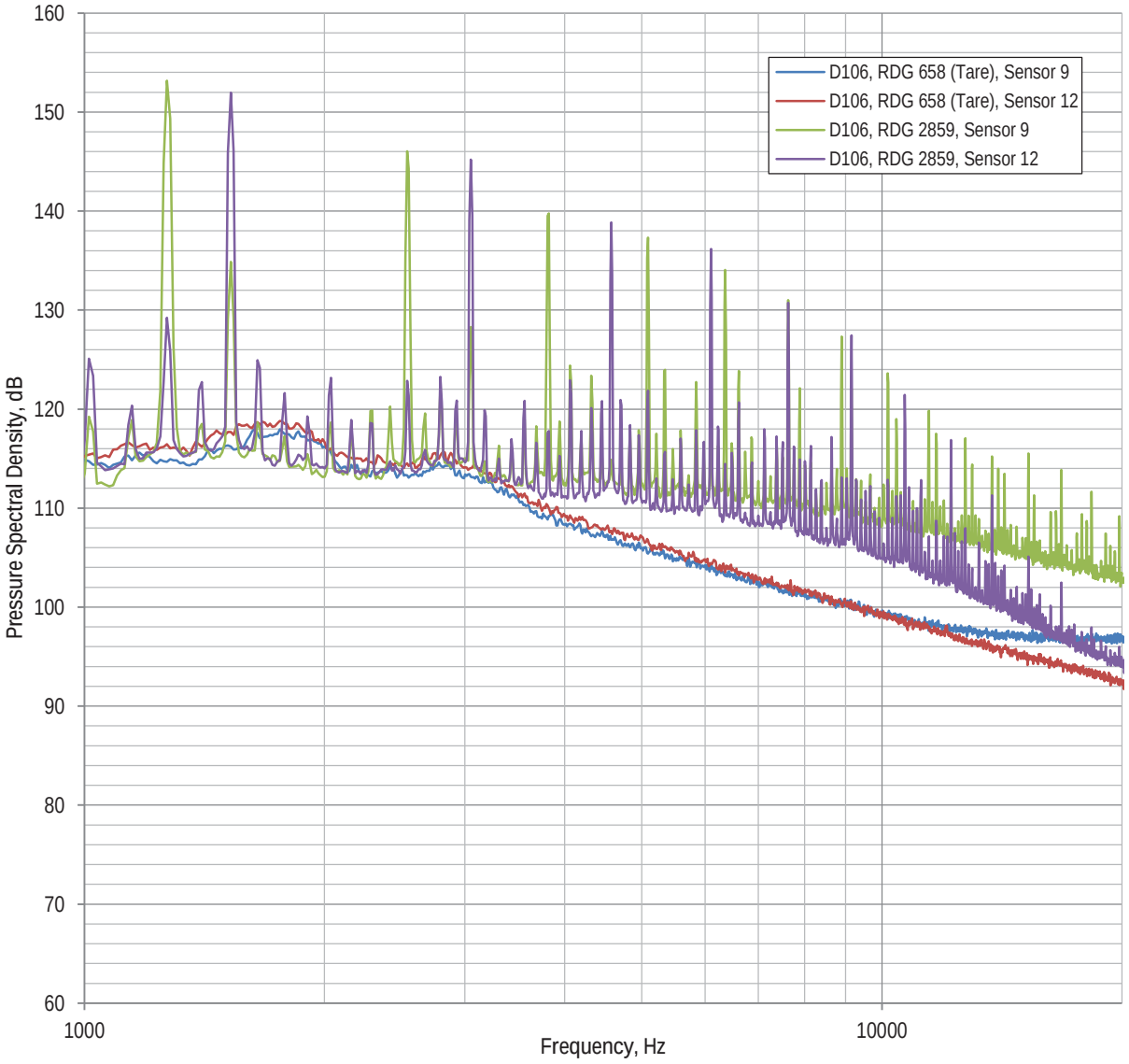

Figure 55.—Sample spectra from 8- by 6-ft SWT.

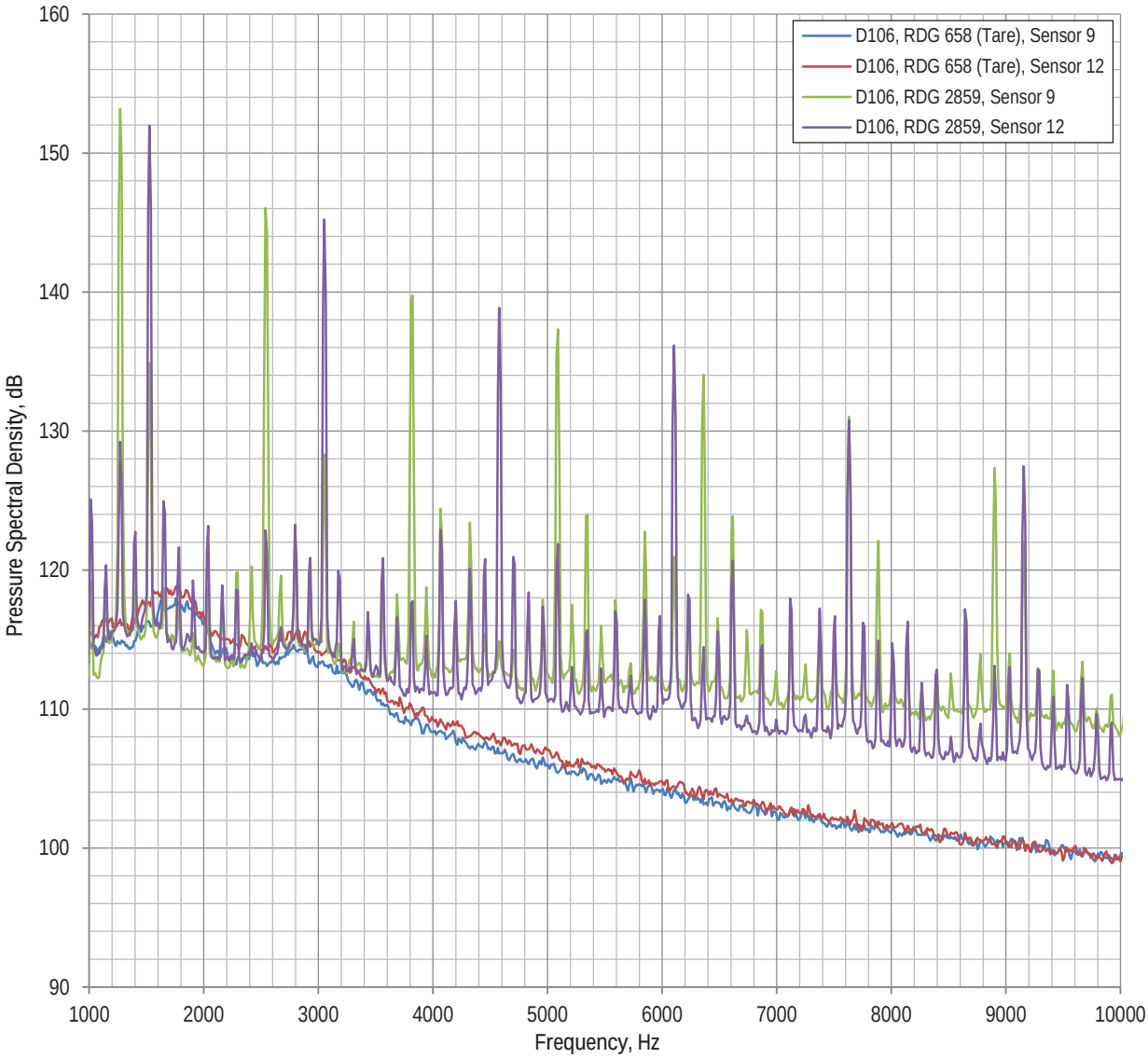

Figure 56.—Sample spectra from 8- by 6-ft SWT (zoomed).

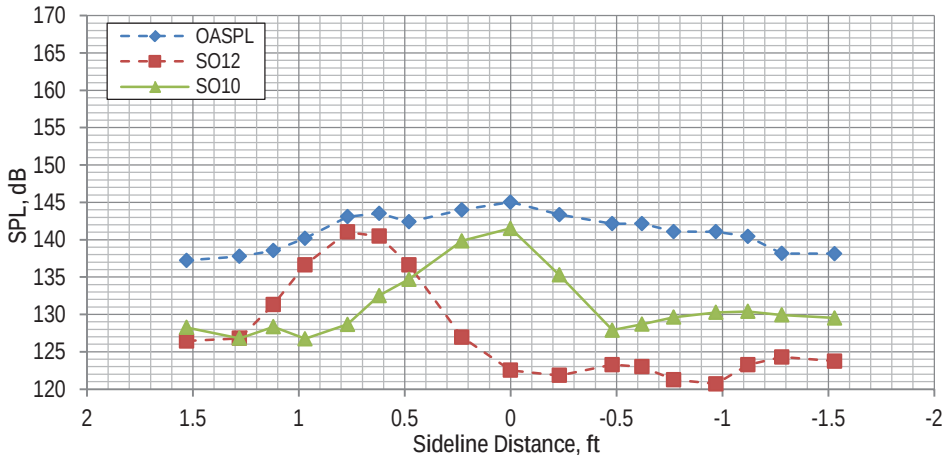

Figure 57.—Blade rate tone levels versus sideline distance, M = 0.27, 43.0/43.5, 771 lbf thrust, D106 RDG 770.

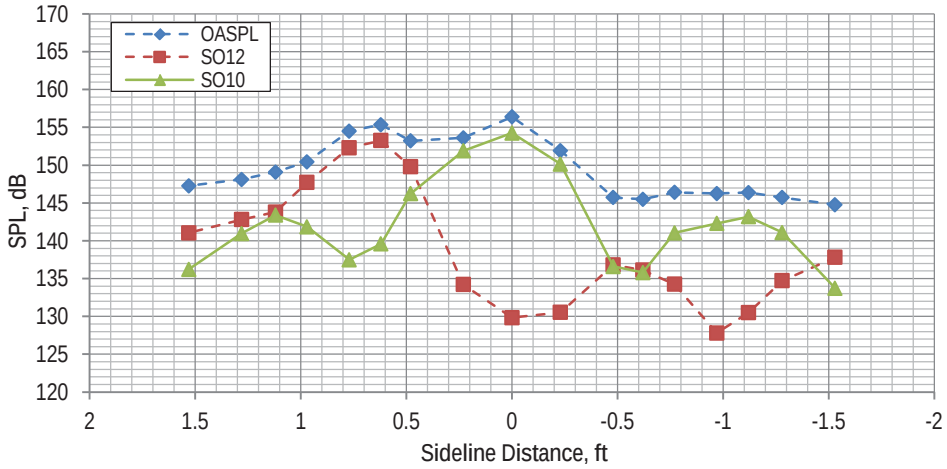

Figure 58.—Blade rate tone levels versus sideline distance, M = 0.60, 54.1/53.5, 552 lbf thrust, D106 RDG 1386.

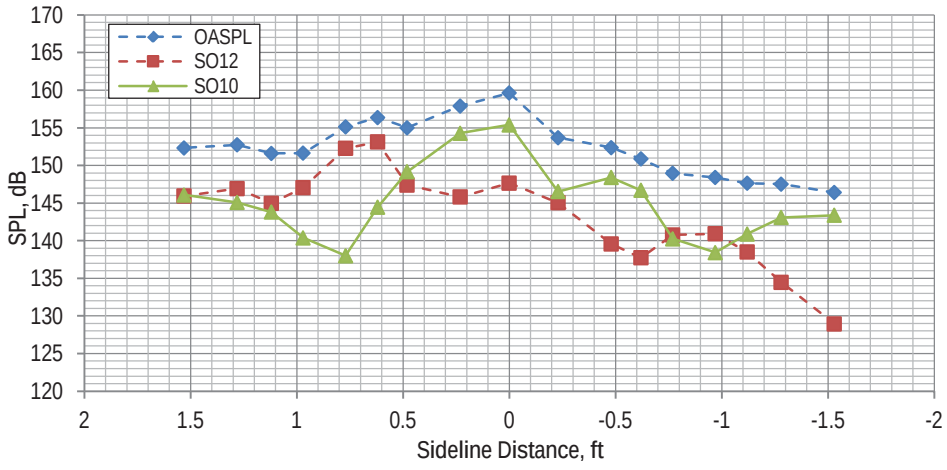

Figure 59.—Blade rate tone levels versus sideline distance, M = 0.67, 60.5/59.0, 642 lbf thrust, D106 RDG 1475.

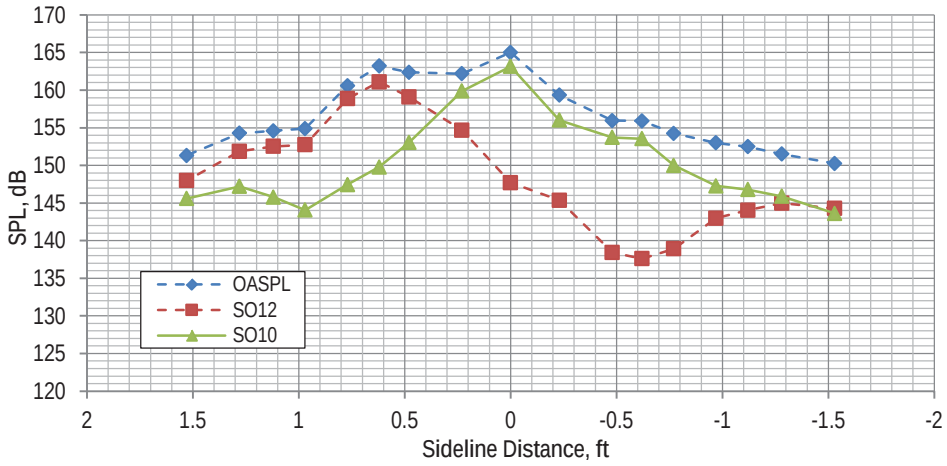

Figure 60.—Blade rate tone levels versus sideline distance, M = 0.73, 62.9/60.5, 723 lbf thrust, D106 RDG 3011.

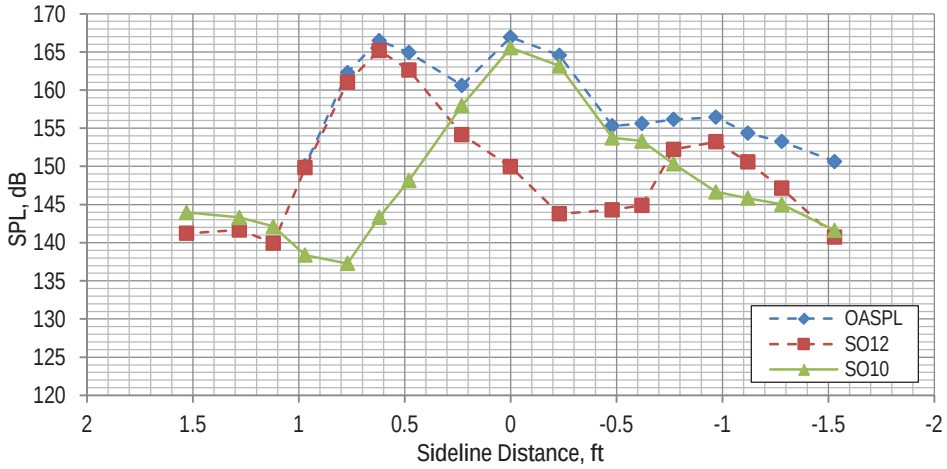

Figure 61.—Blade rate tone levels versus sideline distance, M = 0.78, 62.9/60.5, 762 lbf thrust, D106 RDG 3030.

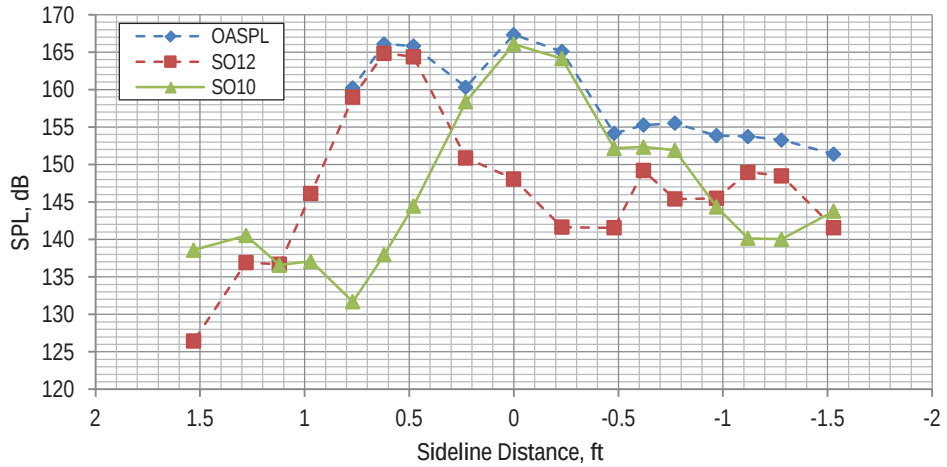

Figure 62.—Blade rate tone levels versus sideline distance, M = 0.80, 62.9/60.5, 747 lbf thrust, D106 RDG 3049.